Faculty of Science
Palacký University Olomouc

Department of Experimental Physics

Master thesis

Nanostructured carbon and metal foils used in mass separator MASHA

Author	Bc. Filippos Georgiadis
Supervisor	doc. RNDr. Jiří Pechoušek, Ph.D.
Degree program	Nanotechnology
Form of study	Full-time
Year	2022

Bibliografická identifikace

Jméno a příjmení autora	Bc. Filippos Georgiadis
Název práce	Nanostrukturované uhlíkové a kovové fólie používané v hmotnostním separátoru MASHA
Typ práce	diplomová
Pracoviště	Katedra experimentální fyziky
Externí pracoviště	Společný ústav jaderných výzkumů v Dubně
Vedoucí práce	doc. RNDr. Jiří Pechoušek, Ph.D.
Konzultant	Vladimir Alexeevich Skuratov, Ds.C.
Externí vedoucí	Mgr. Luboš Krupa, Ph.D.
Rok obhajoby práce	2022
Počet stran	66
Počet příloh	1
Jazyk	anglický
Abstrakt	Práce se zabývá analýzou uhlíkových, hliníkových, niklových a titanových fólií, které byly použity při experimentu E0919 na hmotnostním seperátoru MASHA, který se nachází v Spojeném Ústavu Jaderných Výzkumů v Dubně v Ruské Federaci. V této práci analyzuji fólie před a po ozáření iontovým svazkem z cyklotronu U-400M, kde byly urychlovány atomy argonu. Kovové fólie byly použity v *degraderu*, kde snižovali energii vstupujícího svazku. Některé hliníkové fólie se kvůli jejich nízké tloušťce nepodařilo zachránit, protože se propálily. Niklové a titanové fólie prokázali vyšší odolnost, protože se podařilo všechny zachovat bez výrazného poškození. Dále svazek pokračoval do samariového nebo erbiového (podle aktuálního nastavení) terče, kde docházelo ke kolizi a nově vzniklé produkty pokračovaly do *Hot Solid-State Catcher*, kde byly umístěny uhlíkové fólie, které sloužili k adsorpci produktů a jejich následné desorpce, kde ztratily veškerou energii a byly detekovány na detektorech.
Klíčová slova	U-400M, uhlíkové nanostruktury, grafen, uhlíkové nanotrubky, titanové fólie, niklové fólie, hliníkové fólie, ultra-tenké fólie, urychlovač, cyclotron, hmotnostní separátor supertěžkých atomů, ozářené vzorky

Bibliographical identification

Author's first name and surname	Bc. Filippos Georgiadis
Title	Nanostructured carbon and metal foils used in mass separator MASHA
Type of thesis	master
Department	Department of Experimental Physics
External laboratory	Joint Institute of Nuclear Research Dubna
Supervisor	doc. RNDr. Jiří Pechoušek, Ph.D.
Consultant	Vladimir Alexeevich Skuratov, Ds.C.
External tutor	Mgr. Luboš Krupa, Ph.D.
Year of presentation	2022
Number of pages	66
Number of appendices	1
Language	english
Abstract	The thesis is focused on analysis of carbon, aluminum, nickel and titanium foils, which were used in experiment E0919 on the mass separator MASHA, which is located at the Joint Institute of Nuclear Research in Dubna in the Russian Federation. In this thesis, I analyzed foils before and after irradiation by ion beam from the U-400M cyclotron, where argon atoms were accelerated. The metal foils were used on *degrader*, where they reduced the energy of the incoming beam. Some aluminum foils could not be saved due to their low thickness because they burned. Nickel and titanium foils are more durable, as they have all been saved without significant damage. Furthermore, the beam continued to a samarium or erbium (according to the current setting) target, where a collision occurred and the newly formed products continued to *Hot Solid-State Catcher*, where carbon foils were placed, which were used to adsorb products and their subsequent desorption, where they lost all energy and were detected on detectors.
Keywords	U-400M, carbon nanostructures, graphen, carbon nanotubes, titan foils, nickel foils, alluminium foils, ultra-thin foils, accelerator, cyclotron, mass analyzer of super heavy atoms, irradiated foils

Declaration

I declare that this Diploma thesis has been elaborated by me personally under the supervision of doc. RNDr. Jiří Pechoušek, Ph.D. and, to the best of my knowledge and belief, it contains no material previously published or written by another person, except where due reference is made in the text of the thesis.

In Olomouc on .....

.....
signature

I would like to thank my supervisor doc. RNDr. Jiří Pechoušek, Ph.D. for carrying out my master thesis in cooperation with the Joint Institute for Nuclear Research (JINR) in Dubna in the Russian Federation. I would like also thank Mgr. Luboš Krupa, Ph.D. and all Russian colleagues for their kind approach to working at the MASHA (Mass Analyzer of Super Heavy Atoms)control panel. Mgr. Antonín Opíchal deserves a huge thank not only for his help with administrative staffs upon my arrival at the JINR, but especially for his help in processing the data from the 2019 experiment. I would like to thank Mgr. Pavel Kohout, Ph.D. and Mgr. Alena Kohoutová for being able to share a study with them for half year at the future MR-TOF (multi-reflection time-of-flight) control pannel, where they were both helpful to me in all directions. Also thanks to Vladimir Alexeevich Skuratov, D.Sc. for assistance in material research of irradiated foils and also his colleague Mgr. Ekaterina Korneeva, Ph.D. for the implementation of measurements and consultation of measurement results. My thanks for doc. Mgr. Vít Procházka, Ph.D. for measuring foils by X-ray diffraction. Also i would like to thank Mgr. Vítězslav Heger for fast measuring on SEM. Also I would like to thank to Klára Košnovská for emotional support.

Contents

Introduction

This work is focused on the material analysis of foils that were used in the Mass Analyzer of Super Heavy Atoms (MASHA), which was the content of my internship at Flerov Laboratory for Nuclear Reactions at Joint Institute for Nuclear Research in Russia. The whole work consists of several parts, which are not only in the main part but also in the appendix. It was necessary to fragment the individual data into several dozen files and calculate the fluences and make a correction according to faraday cap (F2C), which was successful with Experiment I (EXP I). For Experiment II (EXP II), faraday cap (F2C) has stopped working and therefore the fluctuations for Experiment II are inaccurate. The individual foils removed from the safe were not described and most of the described foils were helped by my colleagues on the MASHA (Mass Analyzer of Super Heavy Atoms) control panel. The Experiment II (EXP II) foils were removed from the degrader and described. SEM, EDX and XPS analysis was performed in cooperation with the nanolaboratory at Flerov Laboratory for Nuclear Reactions. After returning from my internship, I initiated additional measurements at Palacký University at the Department of Experimental Physics. Additional measurement methods include an Olympus digital microscope, XRD, SEM and EDS analysis.

1 Theoretical part

1.1 Cyclotron U-400M

The isochronous U-400M cyclotron is in operation since 1991. Main tasks of cyclotron U-400M are producing of radioactive ion (fig.1) beams (RIBs), reactions with exotic nuclei and study properties and structure of light exotic nuclei. The cyclotron was originally intended for acceleration ion beams with energies of 34/50 MeV/nucleon and $A/Z = 3/3.6$, where A is atomic weight of the accelerated ion and Z is ion charge when accelerated. At the beam extraction is used stripping foil method. In 2008 the cyclotron possibilities have been extended by additional ion beams with $A/Z = 8/10$ at energies of 4.5/9 MeV/nucleon and it opened new door for synthesis the new super heavy elements and applied research. In the cyclotron U-400M is used superconducting Dubna ECR Ion Source (DECRIS-SC2). The beam is focused by solenoidal lens. It is situated between the ECR and 90° magnet. According to fig.2 is possible to see outputs from cyclotron U-400M to specific experiments, for example MASHA, ACCULINNA-1, ACCULINA-2 and COMBAS. [1, 2, 3]

Ion	Ion energy [MeV/A]	Output intensity	Ion	Ion energy [MeV/A]	Output intensity
^{7}Li	35	6×10^{13}	^{58}Fe	5	3×10^{12}
^{18}O	33	1×10^{13}	^{124}Sn	5	2×10^{11}
^{40}Ar	40	1×10^{12}	^{136}Xe	5	4×10^{11}
^{48}Ca	5	6×10^{12}	^{238}U	7	2×10^{10}
^{54}Cr	5	3×10^{12}			

Figure 1 | Table with specific ion of beam line, ion energy values and output intensities for different nucleis edited and obtained from [2]

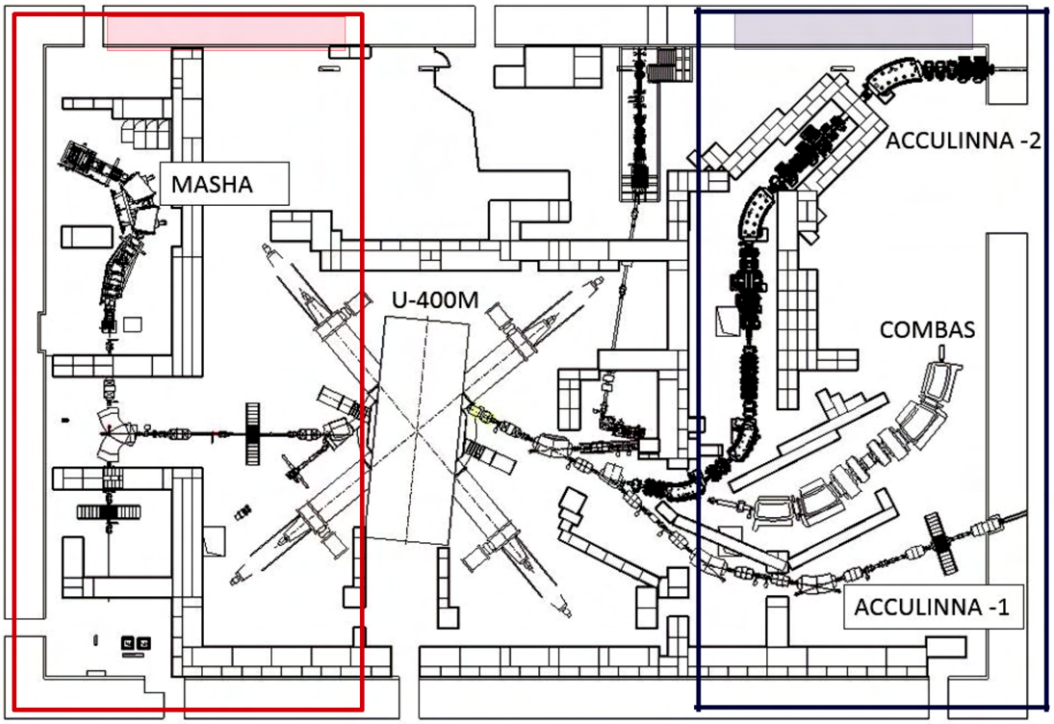

Figure 2 | Schema of U-400M setup obtained from [2]

1.2 Mass Analyzer of Super Heavy Atoms (MASHA)

MASHA (Mass Analyzer of Super Heavy Atoms) is based on the beam line of Cyclotron U-400M (fig.2) at Flerov Laboratory of Nuclear Reactions (FLNR) at Joint Institute for Nuclear Research (JINR), Dubna, Russia. Constructed as the mass-spectrometer in a large variety of masses (from 1 to 450 a.m.u.) and for on-line measurements of the physical properties of superheavy elements (SHE), such as decay energy and modes, mass and half- lives. MASHA is used for a fundamental investigations in nuclear physics. The MASHA setup (fig.3) is a combination of the ISOL (Isotope Separation On-Line) method of synthesis and separation of radioactive nuclei with the classical magneto-optical mass analysis, allowing mass identification of the synthesized nuclides in the wid range of masses. MASHA was related to study the neutron-rich nuclei near the N=126 neutron shell closure. These nuclei were planned to be produced in the multi-nucleon transfer reactions with mass-to-charge ratio separation of the target like fragments. This had to be in favor of increasing the yield of newborn nuclei. It was also expected that a prior determination of masses of the nuclei under investigation will essentially facilitate the analysis of their decays with using the hybrid pixel detectors of the TIMEPIX type. These detectors have a high spatial and energy resolution and allow one to count a single β- or α-particle.[5, 6, 7, 8, 9]

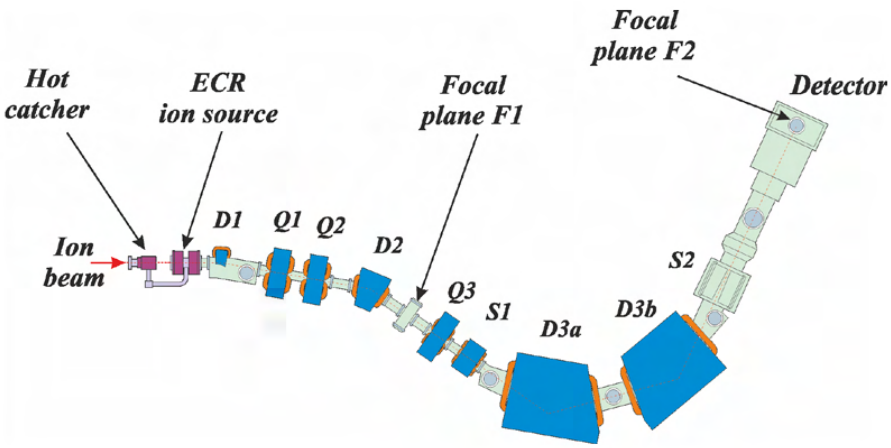

Figure 3 | Schema of MASHA setup obtained from MASHA group

1.2.1 Ion-optical layout

A magneto-optical mass-to-charge ratio analyzer includes four dipole magnets (D1, D2, D3a, D3b), three quadrupole lenses (Q1, Q2, Q3), two sextupole lenses (S1, S2) and a focal plane detector system. [5, 6, 7]

1.2.2 ECR ion source

The ECR (Electron Cyclotron Resonance) ion source operates at the microwave generator frequency of 2.45 GHz. The incoming atoms of nuclear reaction products are ionized to the charge state Q=+1 and accelerated to 40 keV by a three-electrode electrostatic lens. The ion beam formed is separated by the magneto-optical mass-to-charge ratio analyzer. With this ion source it is possible to get beam currents consisting almost entirely (100 %) of singly-charged ions. The ionization efficiency of about 90 % is obtained even for noble gases. [5, 6, 7]

1.2.3 Targed box

Target system represents a block of rotating targets, assembled into cassettes. The disc rotates at f = 25 Hz and the rotating target was used in this yields to higher efficiency and heat distribution. The ion beam collided with the target and then the reaction products are stopped in catcher. [5, 6, 7]

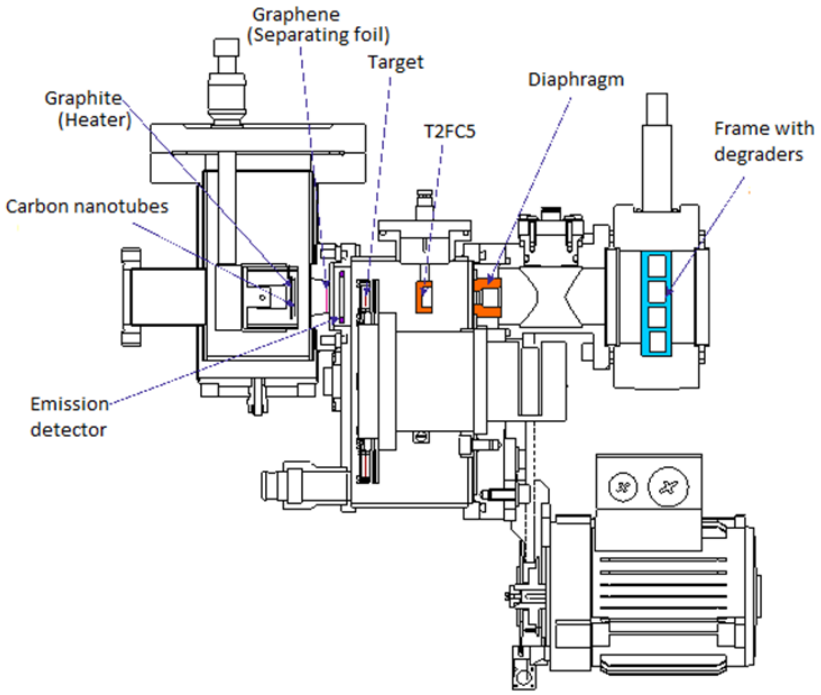

Figure 4 Schema of target box included with hot solid catcher edited and obtained from [10]

1.2.4 Hot solid catcher

The injection of the complete fusion reaction products to the ECR ion source took place after it stopped inside polygraphene catcher unit. After emission from the target the reaction products passed through the separating foil and stopped in a graphite foil heated up to 1800-2000 K. The nuclear reaction products diffused in the form of atoms from the graphite into the vacuum volume of the hot solid catcher. Moving along the vacuum pipe they reached the ECR ion source. [5, 6, 7]

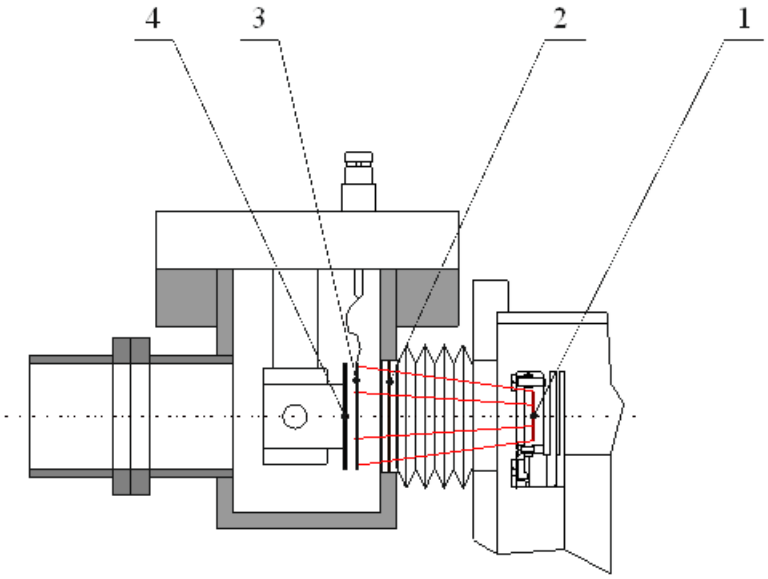

Figure 5 Scheme of hot solid catcher; 1. Target sector on Ti surface; 2. Separating foil (Graphene 300 μm/cm^2); 3. Graphite absorber (Carbon nanotubes graphene)-1,5 mg/cm^2; 4. Graphite foil 50 mg/cm^2 (Heater) obtained from [10]

1.2.5 Detectors and control systems

For detection of nuclear reaction products a multiple detectors system at the focal plane of the mass-separator was installed. The front detector was a multi-strip silicon structure fixed on the surface of glass-cloth laminate. It had an area of 240 x 35 mm^2 and consisted of 192 strips with a pitch of 1.25 mm. The detectors on righ and left side had 16 strips and upper and lower detectors had 64 strips. The all detectors had 300 μm thickness. They were used to determine the energies of the α emmition and the spontaneous fission.
The control of the ion-optical elements of the mass-separator, the vacuum system, the ECR ion source and the hot catcher was made on the base of the standard LabVIEW packet with personal computers located in the control room of the MASHA facility. [5, 6, 7]

1.3 Degrader

The degrader is used to reduce the energy of the incoming ion beam. The energy of the argon ion beam accelerated on the U-400M cyclotron was changed using a titanium degrader which is on the same frame as the target. [11]

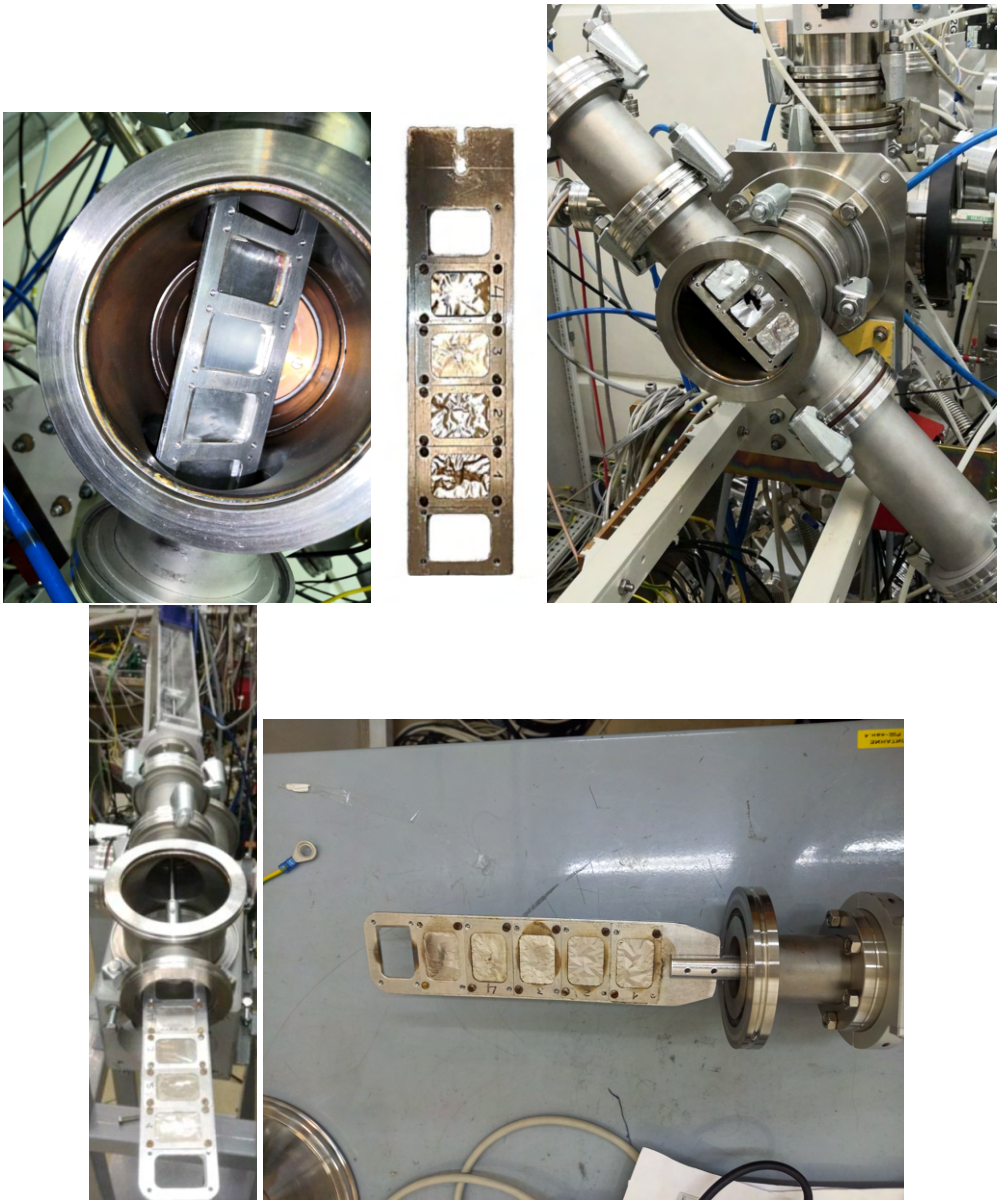

Figure 6 Images of degrader which was used in experiment E0919 and obtained from members of MASHA group.

1.4 High quality multi layer graphene sheets prepared by pyrolysis of thin polyimide films

The key elements of particle accelerators are the charge removal foils, which are used to adjust the charge of the ions to achieve good acceleration. Carbon foils are the most promising candidates due to their low density and excellent thermomechanical properties for accelerators. They can be exposed to high intensity rays. After irradiation with a strong ion beam, carbon foils are subject to deformation, radiation damage and mechanical stress. Another problem is radioactivation. In this respect, the carbon purity of the charge removal films is also a key factor in preventing unwanted radioactivation. Graphite is well known as a thermally stable material with high electrical and thermal conductivity. In contrast to commercially available films, it is possible to prepare high-quality multilayer graphene sheets, which are prepared by pyrolysis of thin polyimide films at temperatures of 2900 - 3000 °C. In the article, they found that the films have high thermal diffusivity, high carbon purity, excellent thickness uniformity and good mechanical properties. All indications are that multilayer graphene sheets have a high potential for charge removal films that have a longer life even when irradiated with the highest intensity ion beam. [13]

1.5 Efficiency of carbon foils in Hot Solid Catcher according to experiment

The stability of the separation efficiency of the mercury and radon isotopes that were produced as a whole was studied by the fusion reaction of ^{40}Ar + ^{144}Sm and ^{40}Ar + ^{166}Er. A new design of a solid heat trap based on a thin carbon foil with an admixture of nanotubes was used in the experiment. At the same time, lifetime tests were performed at 1800 °C at an ion beam current of 0.5 μA. Treatment with a ^{40}Ar ion beam with a current of 0.5p μA on a carbon foils with nanotubes showed stable separation efficiency for 85 hours. The previous version of the fixed hot air trap with a thick carbon absorber reduced the separation efficiency by 6 times in the same time. As we can see at fig.7. [15]

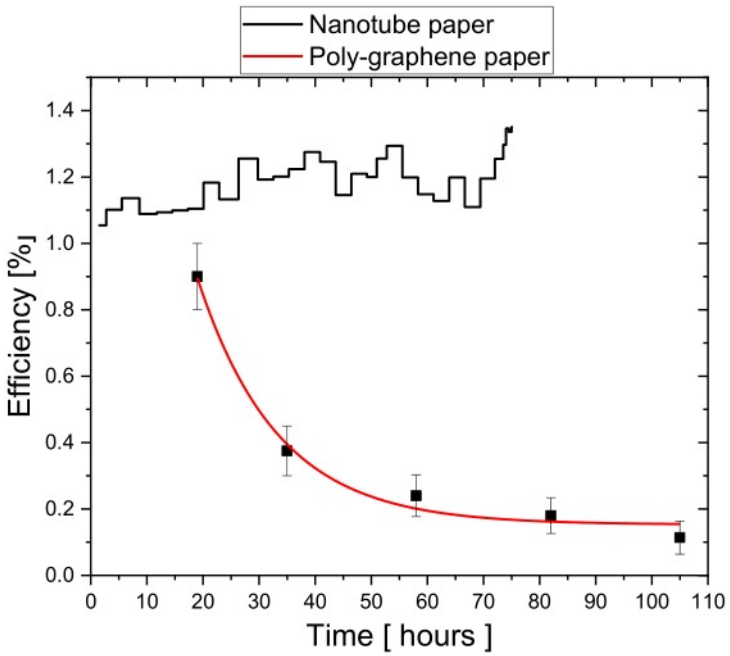

Figure 7 Graph shows different efficiency between two different carbon foils which was used in experiment. The red line at graph is efficiency of poly-graphene paper and black line is efficiency of nanotube paper. The graph has been taken from [15]

2 Experimental part

Experiment E0919 was realized from 05.09.2019 to 25.09.2019 and was divided into two experiment parts. Experiment I has been launched from 07.09.2019 to 15.09.2019 and Experiment II has been launched from 17.09.2019 to 25.09.2019. The main difference between Experiment I and Experiment II was a degrader with different foils. On Experiment I and Experiment II with following marking Experiment I as EXP I and Experiment II as EXP II. In EXP I were analyzed graphene foil from [12] and graphene with mixture of nanotubes from [14]. The foils were analyzed before and after irradiation, where a possible change was observed. In HSC there was the effect of radiation and temperature (around 1800 - 2000 K according to 1.2.4). The degrader is located in front of the hot solid catcher (HSC) as its seen at fig.4 and served primarily to degrade the incoming ion beam. The fluence of all used foils was calculated for EXP I from fig.8 and for EXP II from fig.9 (details of calculations were added at appendix as excel tables 1, 1 in electronic version). There is not temperature detector in the experimental setting (except HSC). The material change could only occur under the influence of temperature and gradual cooling. It didn't have to be due to radiation. This could be due to a combination of temperature and radiation. We cannot say with 100 percent accuracy whether the main factor of change was temperature or irradiation, or a combination of both. Similarly in part EXP II, where nickel and titanium foils were on the degrader. Doses for individual films were also calculated in EXP II, but without correction. The foils in the experiment were exchanged. In EXP I irradiated foil 2.5.5 was by mistake changed for alluminium foil, in EXP II irradiated foil 2.6.2 and irradiated foil 2.6.4 were also changed. In EXP I foils 2.5.3 and 2.5.4 were analyzed because the irradiated foils 2.5.1 and 2.5.2 burned. Foil 2.5.5 was used but there is no mention of its use in the data files and therefore it was not analyzed. In EXP II foil 2.6.5 was not analyzed because, as with EXP I, its used is not mentioned anywhere. Due to the complexity of the whole experiment, an extensive material analysis was performed, thanks to which it was possible to reveal both the low efficiency of the pure graphene film and the confusion and shortcomings of the E0919 experiment. The measuring was realized on two institutes. First SEM, EDS and XPS analysis were realized with cooperation of research department for Ion-implantation nanotechnology and radiation material science at FLNR JINR. Second SEM, EDS, XRD and digital microscopy were realized with cooperation of department of experimental physics on Palacký University.

2.1 Fluence

All fluences were calcuted from raw data by an author. Calculation could be find in appendix (1). In fig.8 the green lines are acquisition stop time, because is really important to calculate with every emmision value.

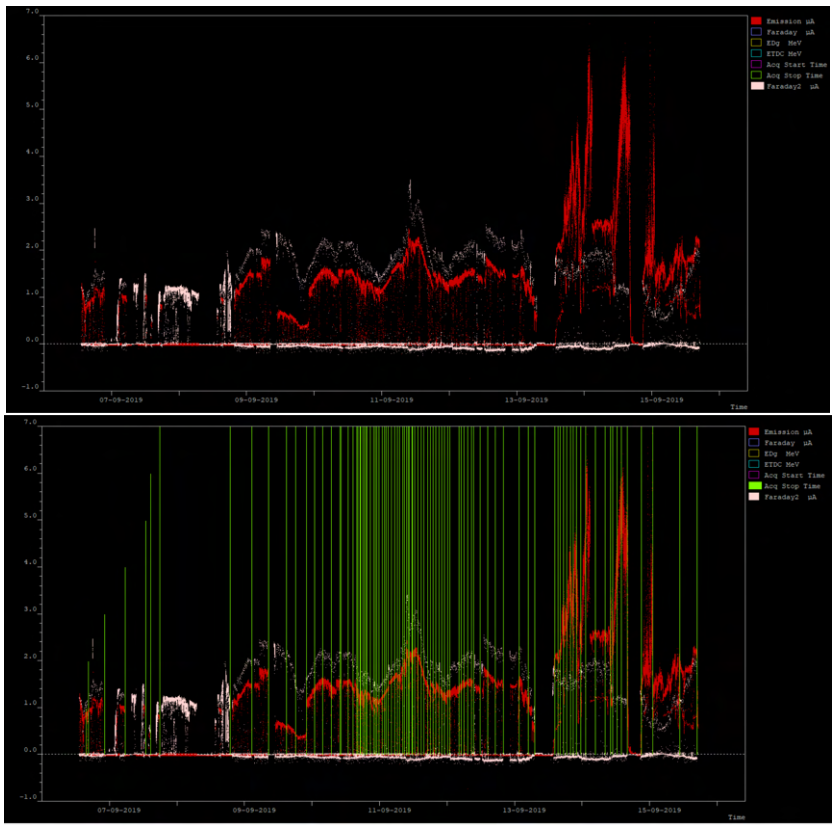

Figure 8 Spectrum of emission energy (red) from emission detector and from faraday cap (white) for EXP I. Green horizontal line divide spectrum on 96 data files.

Expe...	Beam Energy(MeV)	Abs...	Absorber Thick...	Absorber Density (mg/sm2)	Absorber Angle (°)	Absorber 2 Material	Absorber 2 Thickn...	Absorber 2 Density (mg/sm2)	Energy Reaction (MeV)	Energy After ...	Integral (uC)	Regime	C
101	266.000 ±0.4	Ni	4.957	4.41	0.00	Al	1.600	0.43	212.90	181.76	6576.6	10+10	0.
103	267.400 ±0.4	Ni	4.957	4.41	20.00	Al	1.600	0.43	211.47	180.32	5003.5	10+10	0.
104	266.800 ±0.2	Ni	4.957	4.41	27.50	Al	1.600	0.43	207.88	176.70	4239.0	10+10	0.
110	266.500 ±0.2	Ni	4.957	4.41	37.20	Ti	2.000	0.90	201.56	165.65	3975.3	10+10	0.
111	266.500 ±0.2	Ni	4.957	4.41	40.65	Ti	2.000	0.90	198.61	162.65	3979.7	10+10	7
112	266.400 ±0.2	Ni	4.957	4.41	43.60	Ti	2.000	0.90	195.52	159.51	3955.9	10+10	7
113	266.400 ±0.1	Ni	4.957	4.41	46.13	Ti	2.000	0.90	192.57	156.51	1271.8	10+10	6
114	266.500 ±0.4	Ni	4.957	4.41	48.33	Ti	2.000	0.90	189.75	153.64	1535.4	10+10	6
115	267.400 ±0.2	Ni	4.957	4.41	50.35	Ti	2.000	0.90	187.74	151.60	1534.2	10+10	6
116	267.600 ±0.3	Ni	4.957	4.41	52.10	Ti	2.000	0.90	185.04	148.84	1399.3	10+10	7
117	267.580 ±0.7	Ni	4.957	4.41	53.70	Ti	2.000	0.90	182.04	145.78	1473.2	10+10	5
118	267.690 ±0.7	Ni	10.196	9.07	0.00	Ti	2.000	0.90	163.98	127.31	586.0	10+10	5
121	267.680 ±0.5	Ni	10.196	9.07	10.60	Ti	3.0	1.4	162.17	119.67	1574.0	10+10	3
122	267.300 ±0.3	Ni	10.196	9.07	18.60	Ti	3.0	1.4	157.77	115.10	1576.8	10+10	2
123	267.830 ±0.4	Ni	10.196	9.07	23.90	Ti	3.0	1.4	154.34	111.53	1426.5	10+10	1
124	267.000 ±0.9	Ni	10.196	9.07	27.85	Ti	3.0	1.4	149.38	106.36	1141.7	10+10	1
125	267.400 ±0.2	Ti	5.000	2.26	57.55	Ti	3.0	1.4	212.91	171.96	1141.7	3+3	6
126	267.160 ±0.5	Ti	5.000	2.26	55.10	Ti	3.0	1.4	215.61	174.71	1068.9	3+3	3
127	266.600 ±0.4	Ti	5.000	2.26	52.15	Ti	3.0	1.4	218.00	177.16	1327.0	3+3	2
128	267.000 ±0.5	Ti	5.000	2.26	48.50	Ti	3.0	1.4	221.48	180.71	1615.1	3+3	2
129	266.800 ±0.4	Ti	5.000	2.26	44.00	Ti	3.0	1.4	224.26	183.55	1786.0	3+3	2
130	266.830 ±0.3	Ti	5.000	2.26	38.20	Ti	3.0	1.4	227.23	186.58	2210.1	3+3	1
131	266.800 ±0.3	Ti	5.000	2.26	29.70	Ti	3.0	1.4	230.22	189.63	2141.1	3+3	1
132	267.200 ±0.3	Ti	5.000	2.26	13.80	Ti	3.0	1.4	233.65	193.12	1174.3	3+3	1
133	266.490 ±0.4	Ti	5.000	2.26	0.00	Ti	3.0	1.4	233.64	193.11	3228.3	3+3	8
134	266.510 ±0.3	Ti	3.000	1.36	0.00	Ti	3.0	1.4	243.46	203.10	615.4	3+3	1
136	266.500 ±0.7	Ti	3.000	1.36	0.00	Ti	3.0	1.4	243.45	203.09	1196.7	3+3	7
137	265.850 ±0.3	Ti	3.000	1.36	33.40	Ti	3.0	1.4	239.88	199.46	3500.3	3+3	0.
138	266.400 ±0.3	Ti	3.000	1.36	33.40	Ti	3.0	1.4	240.45	200.04	3074.5	3+3	0.
142	266.500 ±0.6	Ni	10.196	9.07	32.17	Ti	3.0	1.4	143.36	100.08	1402.5	3+3	2
143	266.120 ±0.2	Ni	10.196	9.07	34.80	Ti	3.0	1.4	138.94	95.46	2238.4	3+3	2
144	267.890 ±0.6	Ni	10.196	9.07	37.22	Ti	3.0	1.4	137.03	93.46	1840.4	3+3	2
146	267.700 ±0.8	Ti	5.000	2.26	38.20	Ti	3.0	1.4	228.16	187.53	8162.5	3+3	0.
145	268.140 ±0.8	Ti	5.000	2.26	55.10	Ti	3.0	1.4	216.68	175.80	7815.4	3+3	3
141	267.400 ±0.6	Ni	10.196	9.07	32.17	Ti	3.0	1.4	144.48	101.25	356.2	3+3	1
140	0.000 ±0.0	Ni	10.196	9.07	32.17	Ti	3.0	1.4	0.00	0.00	0.0	3+3	0.
139	266.300 ±0.1	Ti	3.000	1.36	33.40	Ti	3.0	1.4	240.35	199.93	0.0	3+3	0.
135	266.600 ±0.3	Ti	3.000	1.36	0.00	Ti	3.0	1.4	243.55	203.19	518.0	3+3	9
120	267.400 ±0.4	Ni	10.196	9.07	10.60	Ti	2.000	0.90	161.83	125.10	0.0	10+10	0.
119	267.400 ±0.4	Ni	10.196	9.07	10.60	Ti	2.000	0.90	161.83	125.10	0.0	10+10	0.
109	266.700 ±0.0	Ni	4.957	4.41	37.20	Ti	2.000	0.90	201.78	165.88	192.1	10+10	0.
108	267.000 ±0.3	Ni	4.957	4.41	37.20	Ti	2.000	0.90	202.12	166.22	1056.0	10+10	2
107	267.500 ±0.5	Ni	4.957	4.41	37.20	Ti	2.000	0.90	202.67	166.78	1615.2	10+10	0.
106	266.700 ±0.2	Ni	4.957	4.41	32.90	Al	1.600	0.43	204.80	173.60	0.0	10+10	0.
105	0.000 ±0.0	Ni	4.957	4.41	0.00	Al	1.600	0.43	0.00	0.00	0.0	10+10	0.
102	266.700 ±0.1	Ni	4.957	4.41	0.00	Al	1.600	0.43	213.66	182.53	977.9	10+10	0.

Figure 9 According to missing spectrum of emission energy here is the table which was obtained from MASHA database, where we can find emission values for every data file for EXP II. Values from emission detector (second column) were used for fluence calculation (details of calculation can be find in appendix 1).

2.2 Commercial used foils and their properties

In this section I will introduce commercial metal and carbon foils which were used in experiment E0919. Also I describe their thickness and fluences. The supplier of titanium foils, which was used in EXP II was HAMILTON PRECISION METALS 1780 ROHRERSTOWN ROAD LANCASTER, PA 17601-2334.

2.2.1 Aluminium foils which were used in EXP I in degrader + titanium foil

List of foils thickness and fluences

1 Aluminium foil with thickness -> 5.87 μm (Fluence = $2.11926 \cdot 10^{17}$ cm^{-2}) (According to fig.33 they were burned)

2 Aluminium foil with thickness -> 9.32 μm (Fluence = $2.18321 \cdot 10^{17}$ cm^{-2}) (According to fig.33 they were burned)

3 Aluminium foil with thickness -> 16.7 μm (Fluence = $1.01207 \cdot 10^{17}$ cm^{-2})

4 Aluminium foil with thickness -> combined with 20.5 μm + 5.87 μm (Fluence = $6.93921 \cdot 10^{16}$ cm^{-2})

5 Titanium foil with thickness -> 2 μm (Not analyzed)

2.2.2 Titanium and nickel foils which were used in degrader EXP II

List of foils thickness and fluences

1 Titanium - (2 μm + 3 μm) - 41.5 mm (Fluence = $1.80415 \cdot 10^{16}$ cm^{-2})

2 Nickel - 14.92 mg/cm^2 (8μm) - 71.5 mm (Fluence = $8.31592 \cdot 10^{15}$ cm^{-2})

3 Nickel - 4.41 mg/cm^2 (5μm) - 101.5 mm (Fluence = $2.486 \cdot 10^{16}$ cm^{-2})

4 Titanium - 1.337 mg/cm^2 (3μm) - 131.5 mm (Fluence = $6.06879 \cdot 10^{15}$ cm^{-2})

5 Titanium - 0.939 mg/cm^2 (2μm) - 161.5 mm (Not analyzed)

2.2.3 Carbon foils which were used in EXP I in Hot Solid Catcher

List of foils thickness and fluences

1 Graphene - 5.0 μm $\pm$ 0.2 μm (Fluence = $4.61122 \cdot 10^{16}$ cm^{-2})

2 Graphene mixture with nanotubes - 1.5 μm (Fluence = $2.61568 \cdot 10^{17}$ cm^{-2})

2.3 Carbon foils and their properties for hot solid catcher

In this section I will introduce company suppliers of carbon foils and their properties.

2.3.1 Multi-Layer graphene (MLG) from KANEKA CORPORATION

Multi-layer graphene was bought from KANEKA CORPORATION around 20. November 2017. Thickness of MLG is 5.0 μm $\pm$ 0.2 μm. Extent of foils is 40$\times$40 mm and was bought 10 pieces. [10]

Company description of GRAPHINITY *„GRAPHINITY is a high thermal conductive graphite sheet that has been developed through our high polymer technologies and ultra heat treatment techniques. This material can spread heat from a heat source quickly, and can decrease the temperature of it.“* [12]

Features

- High thermal conductivity (more than three times as high as copper and six times as high as aluminum)
  $\rightarrow$ GRAPHINITY can spread heat in planar direction, and can suppress a heat spot.
- Light weight: Density about 2 g/cm^3, thickness : 25 μm, 40 μm
- Flexible (withstands repeated bending, R = 2 mm, 180°, more than 10000 times bending)
  $\rightarrow$ Easy to manufacture such as punching and bending.
- High electromagnetic shielding effect
- Extremely low water absorption

Materials	Thermal conductivity [W/mK]	Density [g/cm^3]
GRAPHINITY [1]	1500	2.0
Copper [2]	402	8.9
Aluminium [2]	237	2.7
Polystyrene [2]	0.12	1.0-1.1

Table 1 | Table of thermal conductivity and density obtained from [12]

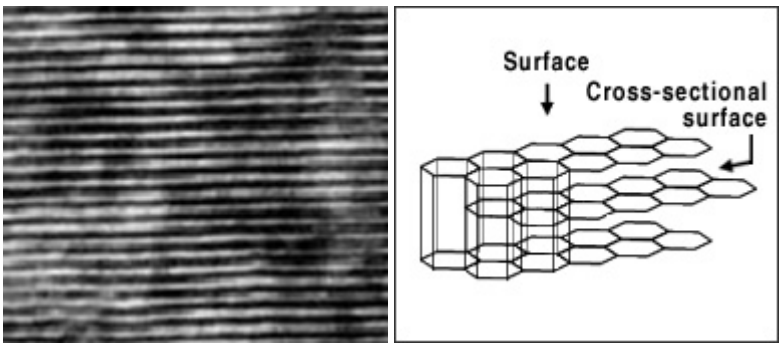

Figure 10 | Cross-sectional TEM image and scheme of graphene structure obtained from [12]

2.3.2 Graphene foils from Applied Nanotech, Inc.

Graphene foils was bought from Applied Nanotech Inc. in 2015. Thickness of graphene foils is around 1.5 μm. Diameter of foils is 4 cm (4.5 from 11) and was bought 5 pieces. The purity is 99.9% and the density is 1.5-2.0 mg/cm^3. [14]

Company description of Graphene foils *„We offer carbon films and foils based on high-strength graphene. Free-standing foils are available made with 100% graphene or with carbon nanotube enhanced graphene (CNT + graphene mixture) for added strength and stiffness. These applications are used on critical components for machines used in medical imaging (such as PET scans).“*[14]

Features

- Long lifetime (exceeding 7.500 μA-hr)
- Custom sizes (up to 26 cm diameter)
- Competitive pricing
- Electrical resistance
- Superior thermal conductivity
- Foil mounting options (bare foils, cut to size, mounted on frames)
- High mechanical strength

Ideal for

- Stripper foil
- Radiation windows
- Gas-cell windows
- X-ray windows
- Ion-beam windows
- Thermal management applications

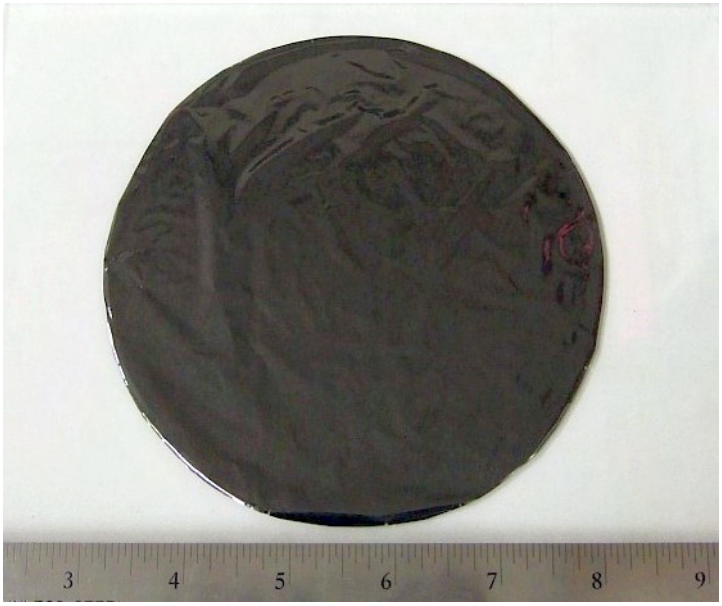

Figure 11 | Example of graphene mixture with nanotubes foil obtained from [14]

2.3.3 List of devices for foil analysis

- SEM and EDX were made on S-3400 N (Hitachi) scanning electron microscope equipped with the Thermo Scientific Ultra Dry EDS detector at 20 kV accelerating voltage [JINR measuring]
- EDS data analysis was made with Thermo Scientific NSS 3.3 software package [JINR measuring]
- XPS was made using a Thermo Fisher K-Alpha spectrometer with monochromatic Al k-alpha X-ray source (providing an energy of 1486.6 eV). The beam spot size is 400 µm and for surface charge neutralization a compensating electron flood gun was used [JINR measuring]
- Scaning Electron Microscopy Tescan Vega 3 [UPOL KEF measuring]
- Olympus digital microscope DSX1000 was used for macro surface pictures with Software OLYMPUS Stream [UPOL KEF measuring]
- Bruker D8 ADVANCE powder diffractometer operated in Bragg-Brentano parafocusing geometry with LYNXEYE position sensitive detector (in 1D mode, angular opening 2.943°) with Co X-ray tube as a radiation source (voltage 35 kV, current 40 mA) with software DIFRAC. EVA v5.1

2.4 Carbon foils for hot solid catcher of EXP I

In this section I analyzed used graphene foils from experiment E0919 from first part of EXP I. The foils were analyzed as pair of nonirradiated and irradiated carbon foils. First will be shown analysis of reference carbon foil and in following figure will be irradiated carbon foil for better clarity.

2.4.1 Multi-layer graphene foil

This section will shown the difference between nonirradiated and irradiated multi-layer graphene, which was used at begining for two days and eneding for two days of experiment Exp I. Calculated fluence value for this multi-layer graphene foil was $4.61122 \cdot 10^{16}$ cm^{-2}.

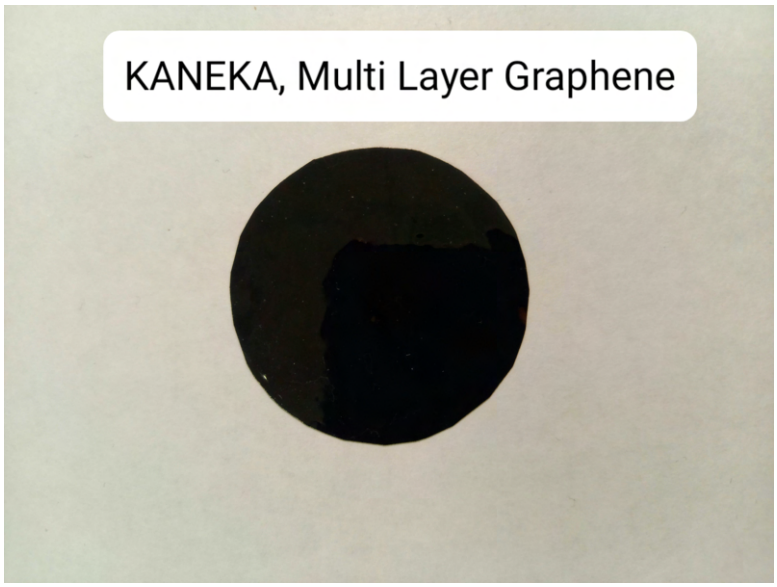

Figure 12 Nonirradiated multi-layer graphene which was bought from KAKNEKA company from Japan according to 2.3.1

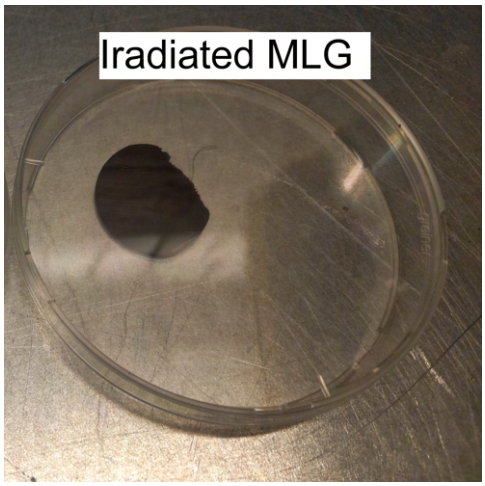

Figure 13 Irradiated multi-layer graphene which was used at MASHA experiment E0919 in Hot Solid Catcher according to journal in appendix 1

At the fig.14 is smooth surface of fig12 with dirt on it. On the other hand the irradiated foil fig.15 of fig.13 is possible to see crumpled surface, which was caused by incoming ion beam, by heat which was conducted from graphite foil in close proximity in hot solid catcher and by manipulation with it.

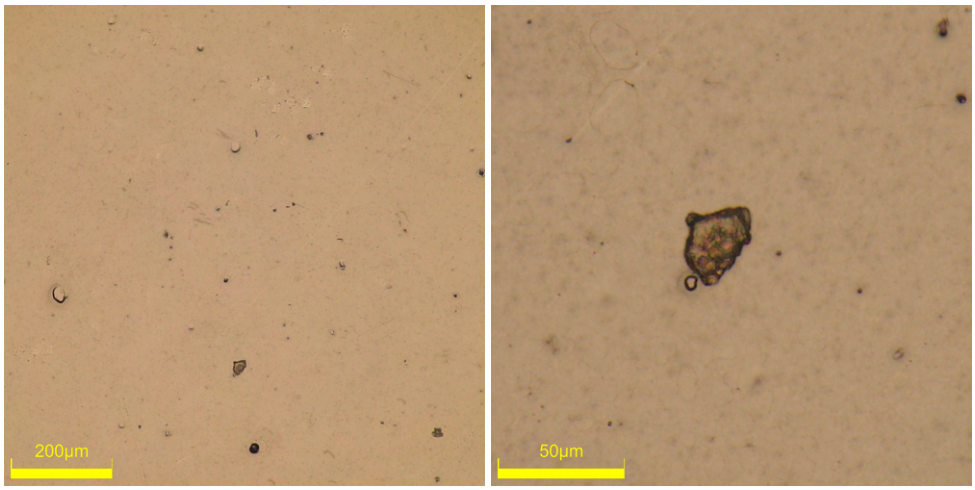

Figure 14 Nonirradiated multi-layer graphenes surface measured by Olympus digital microscope DSX1000 in brightfield (BF) mode in different scale (200 and 50 μm)

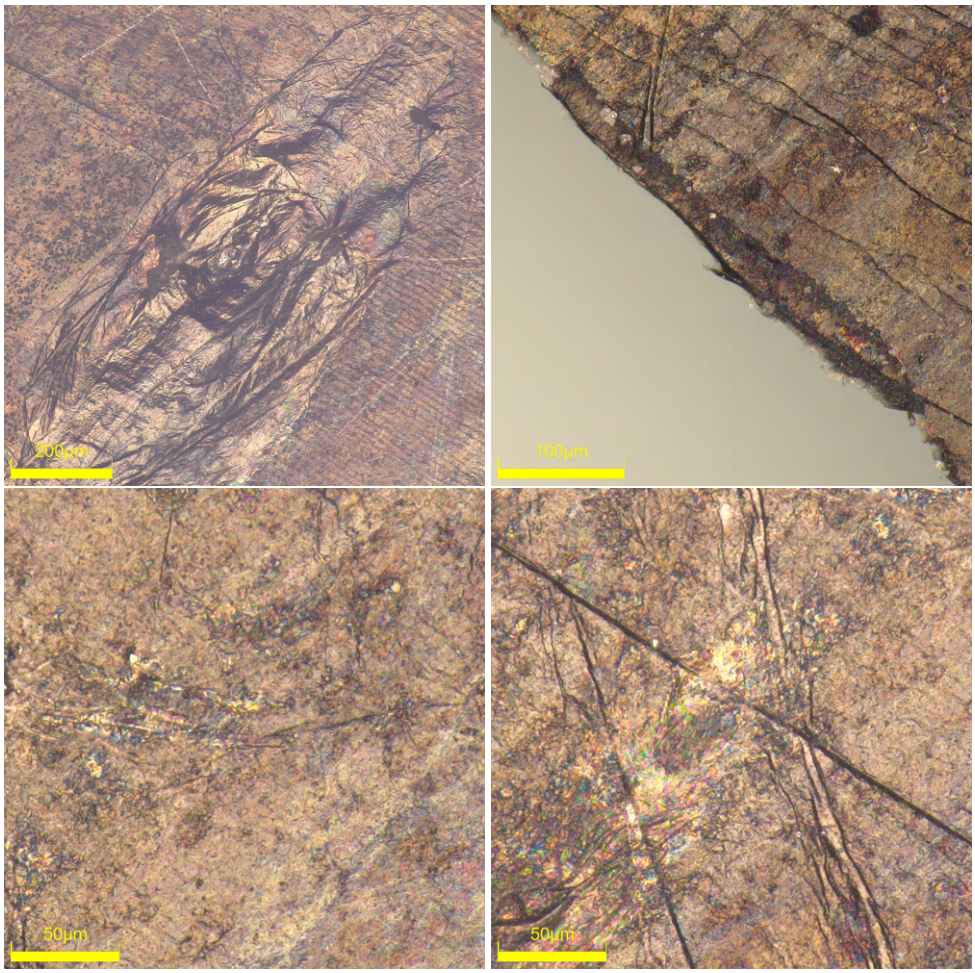

Figure 15 Irradiated multi-layer graphenes surface measured by Olympus digital microscope DSX1000 in brightfield (BF) mode in different scale (200, 100 and 50 μm)

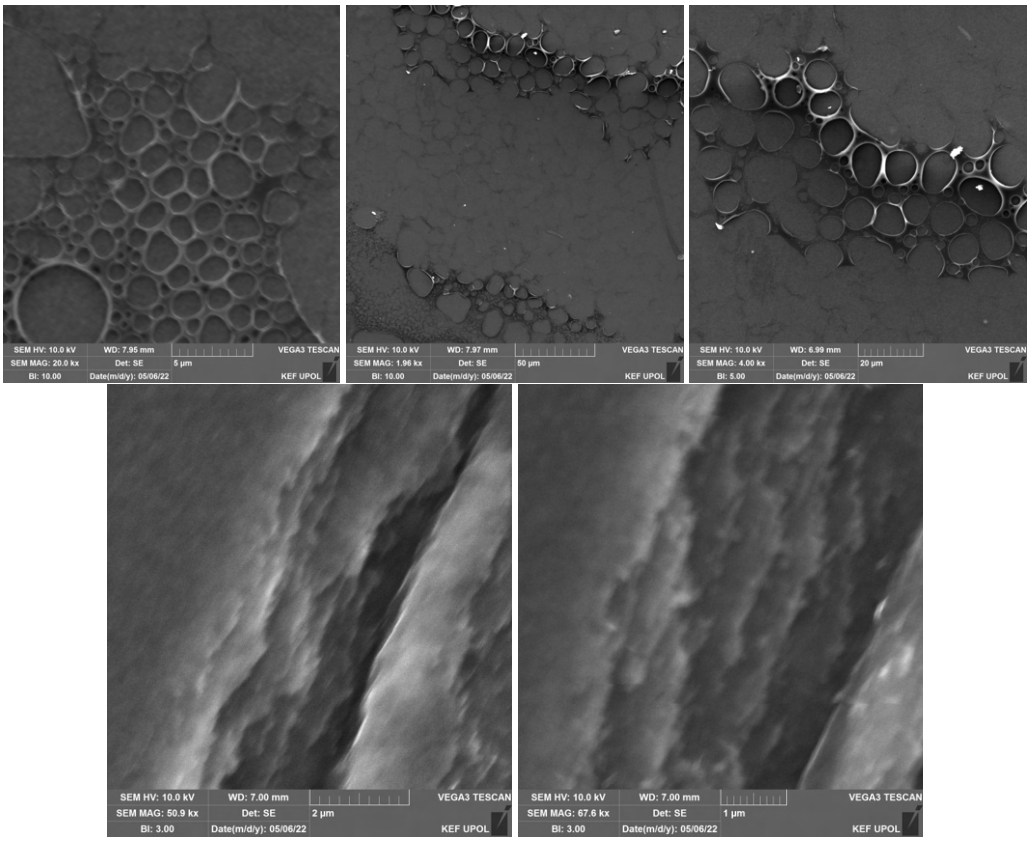

Figure 16 | Nonirradiated multi-layer graphenes surface measured by SEM Tescan Vega 3

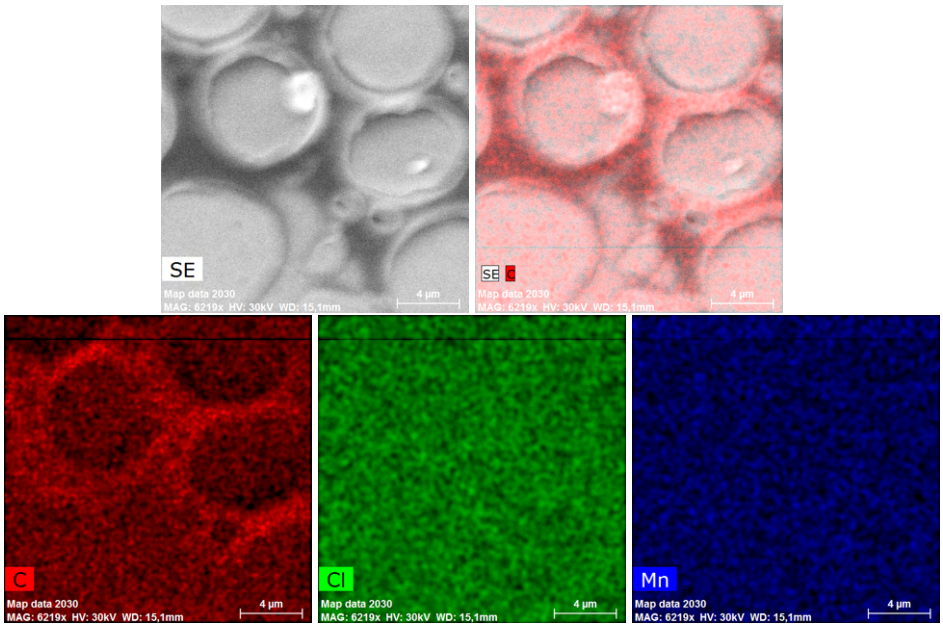

Figure 17 | Nonirradiated multi-layer graphenes surface measured by SEM Tescan Vega 3 in EDS mode for elemental mapping (C, CL, Mn)

At the first three images of the fig.16 is shown matrix as the supplier scheme in fig.10 from polystyrene with containing of chlorine from fig.17. The contamination of matrix by chlorine is also proven by EDS graphs seen in fig.18, where chlorine has the second largest contamination. The last two images of fig.16 shown us the corner of nonirradiated multi-layer graphene foil, where is possible to see the graphene layers.

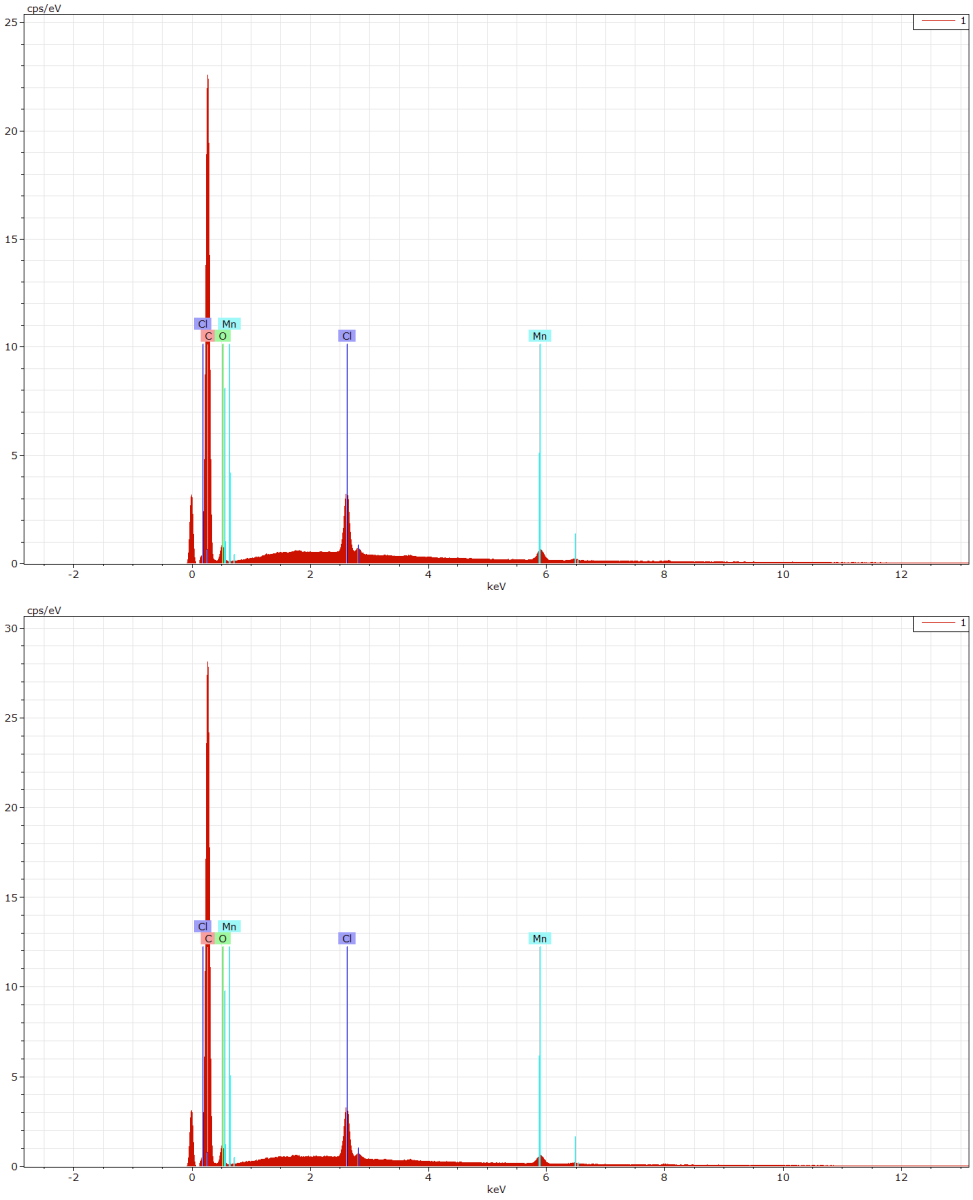

Figure 18 Nonirradiated multi-layer graphenes surface measured by SEM Tescan Vega 3 in EDS mode for elemental mapping as a graph

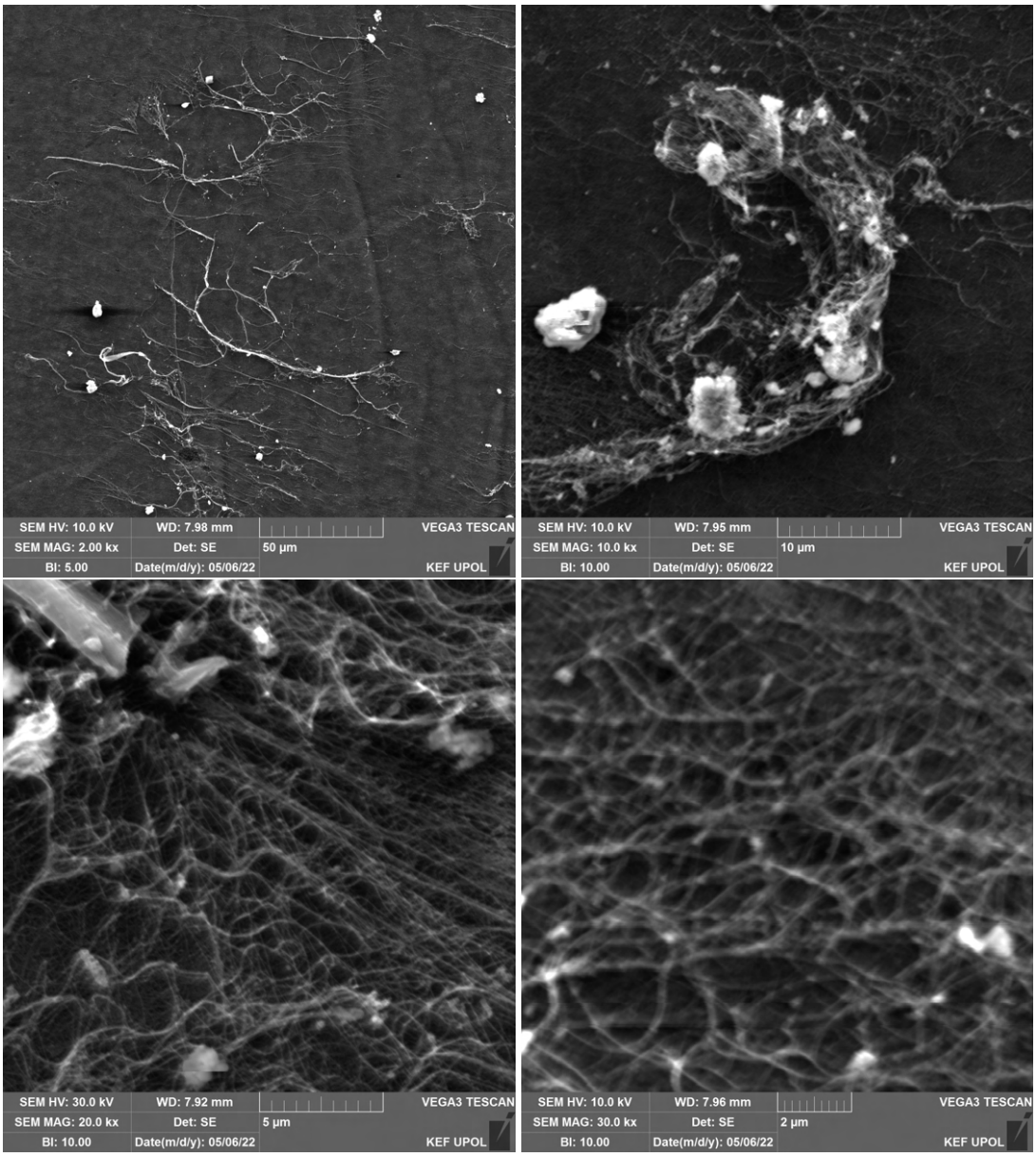

Figure 19 | Irradiated multi-layer graphenes surface measured by SEM Tescan Vega 3

The fig.19 show us the irradiated multi-layer graphene foil (13), where are shown the main changes after irradiation. On the surface grew carbon fibers and the matrix is not possible to find. According to fig.20, where EDS mapping did not shown chlorine content and any other element (higher purity after irradiation). It can cause the reduction of efficiency as is shown in graph 7.

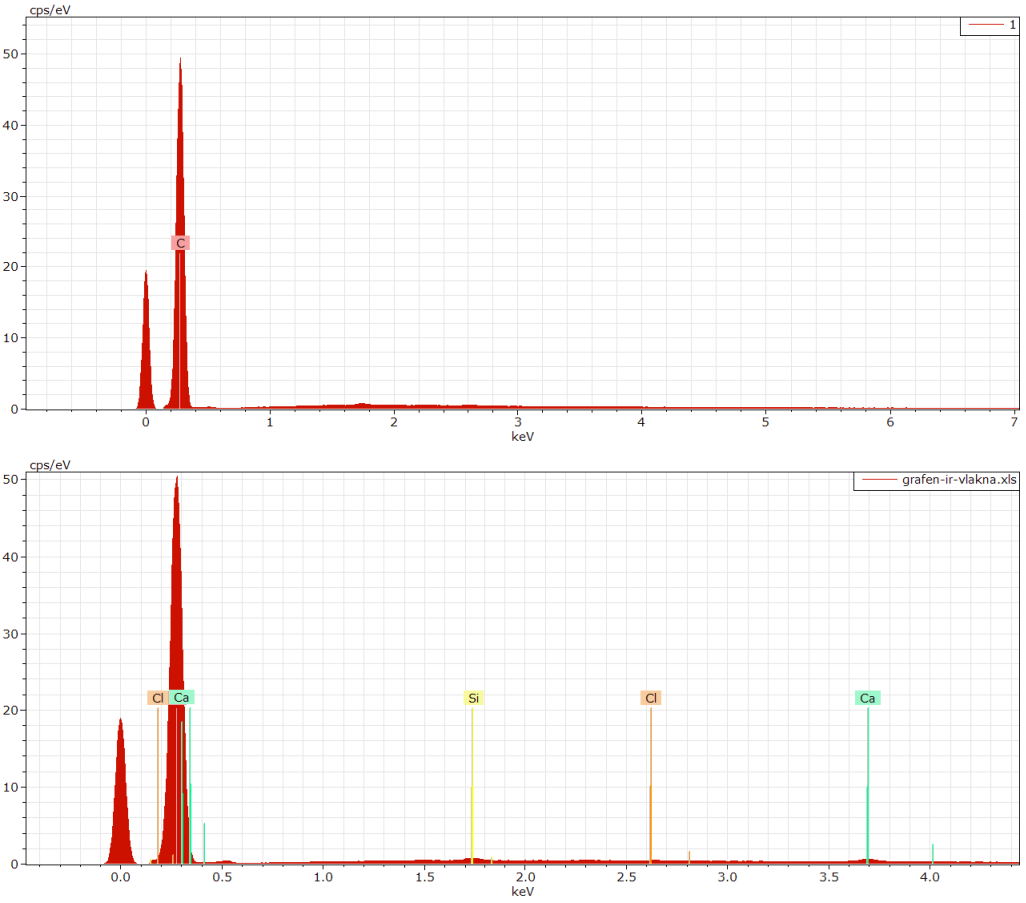

Figure 20 Irradiated multi-layer graphenes surface measured by SEM Tescan Vega 3 in EDS mode for elemental mapping as a graph

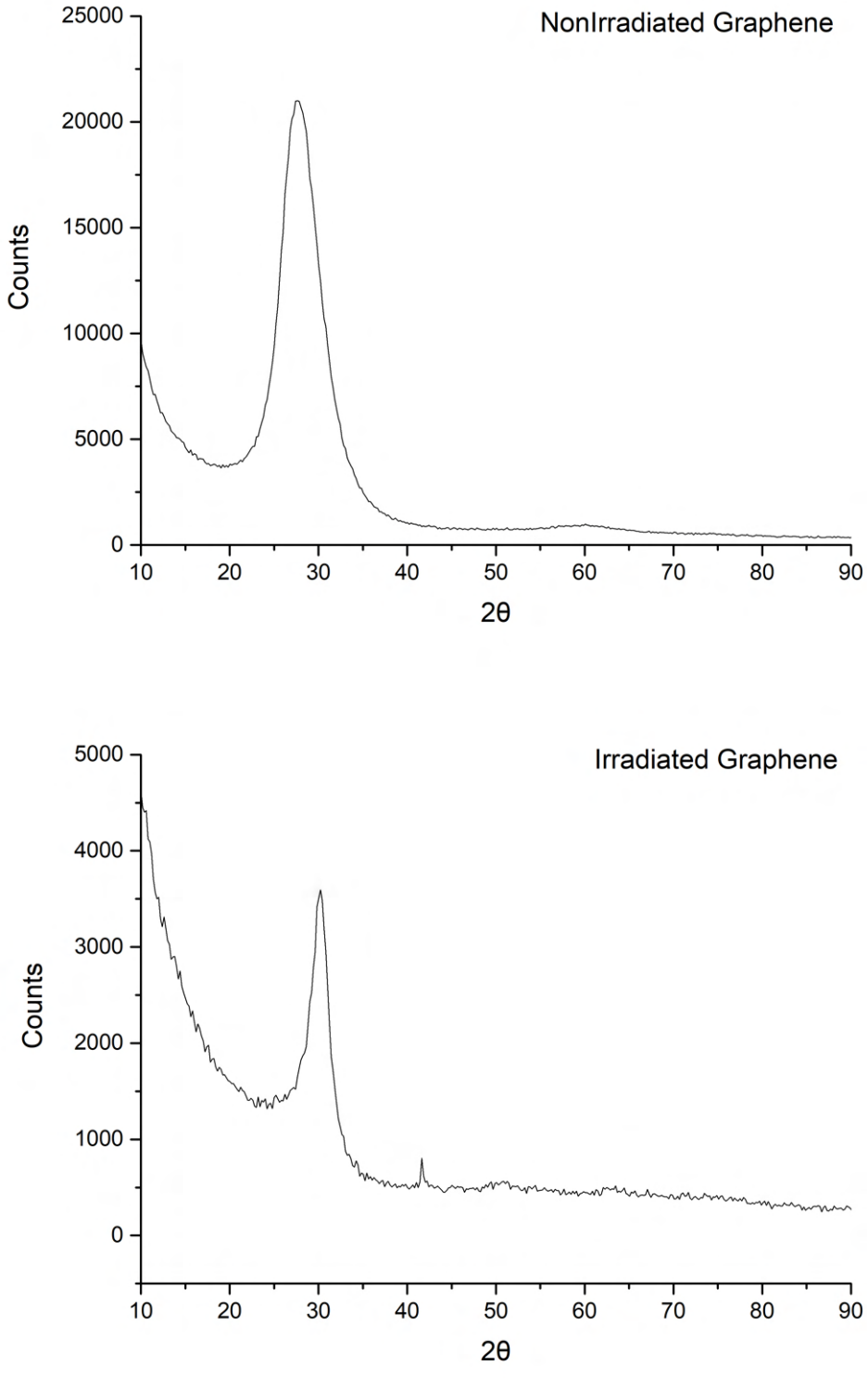

Figure 21 Graphs show us XRD measuring of nonirradiated and irradiated multi-layer graphene foil

XRD at fig.21 and XPS at fig.22 measuring shown us, that there are no large difference changes in crystal structure. Small deviation could be caused by heat or by crumpled surface, where the obtained signal could not be clear.

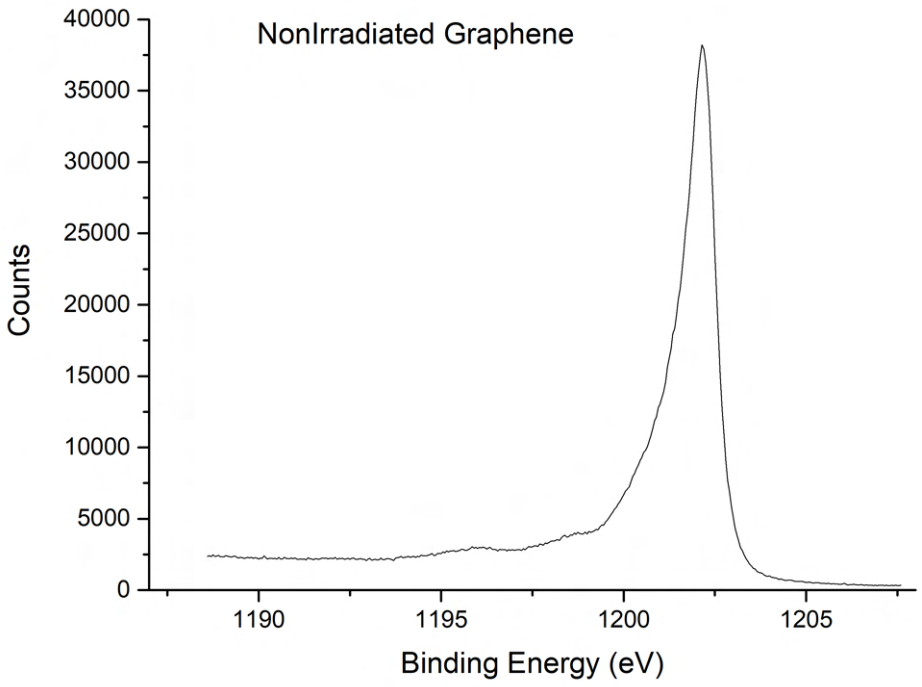

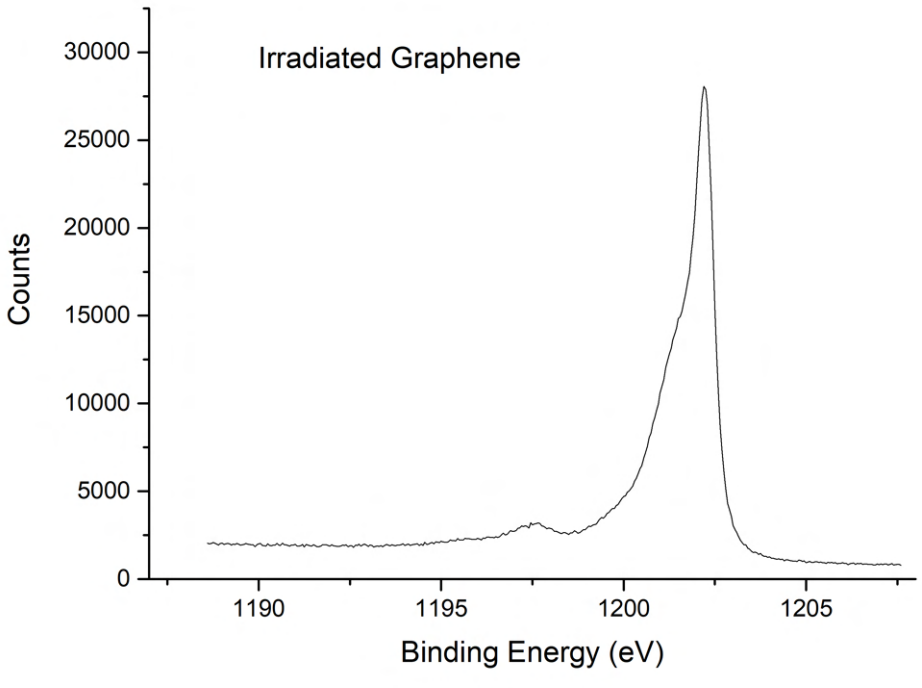

Figure 22 Graphs show us XPS measuring for carbon element of nonirradiated and irradiated multi-layer graphene foil

2.4.2 Graphene foil with mixture of nanotubes

This section will shown the difference between nonirradiated and irradiated graphene mixture with nanotubes, which has been replaced by multi-layer graphene (13). The foil was in experiment Exp I for six days without replacing. Calculated fluence value for this graphene foil with mixture of nanotubes was $2.61568 \cdot 10^{17}$ cm^{-2}.

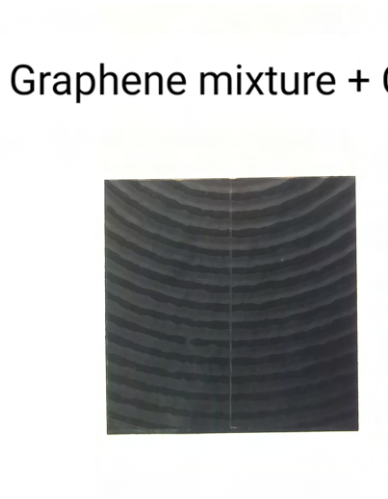

Figure 23 Nonirradiated graphene mixture with nanotubes which was bought from Applied Nanotech, Inc. from USA according to fig.11

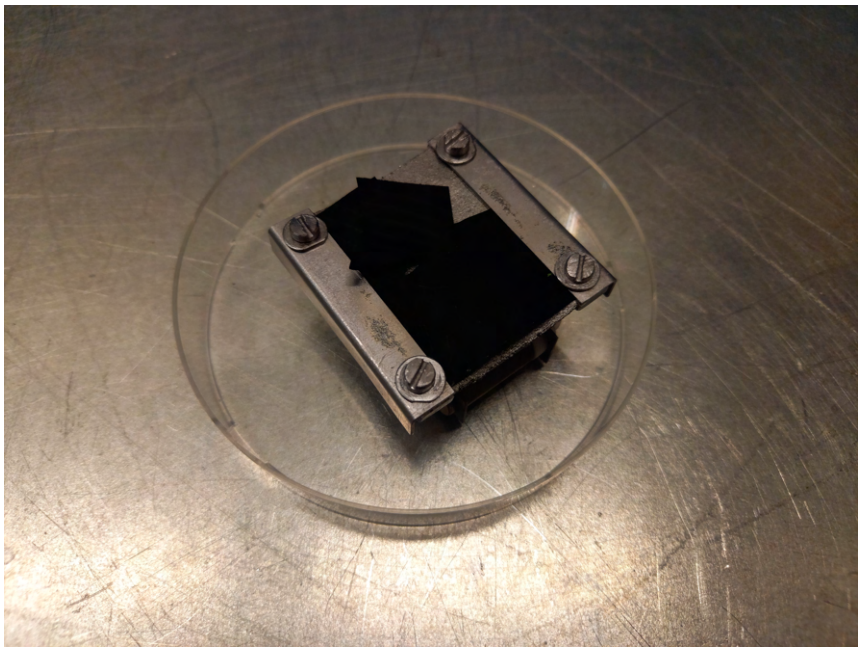

Figure 24 Irradiated graphene mixture with nanotubes still on holder which was used at MASHA experiment E0919 in Hot Solid Catcher according to journal in appendix1. Also is possible to see the silver part of graphite *heater* on holder under graphene foil with mixture of nanotubes

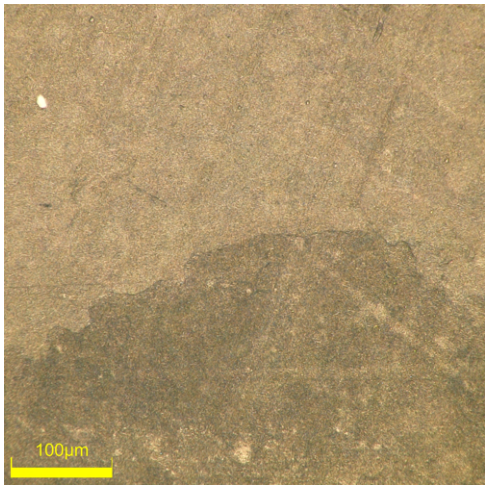

Figure 25 Nonirradiated graphene mixture with nanotubes surface measured by Olympus digital microscope DSX1000 in brightfield (BF) mode in different scale (100 μm)

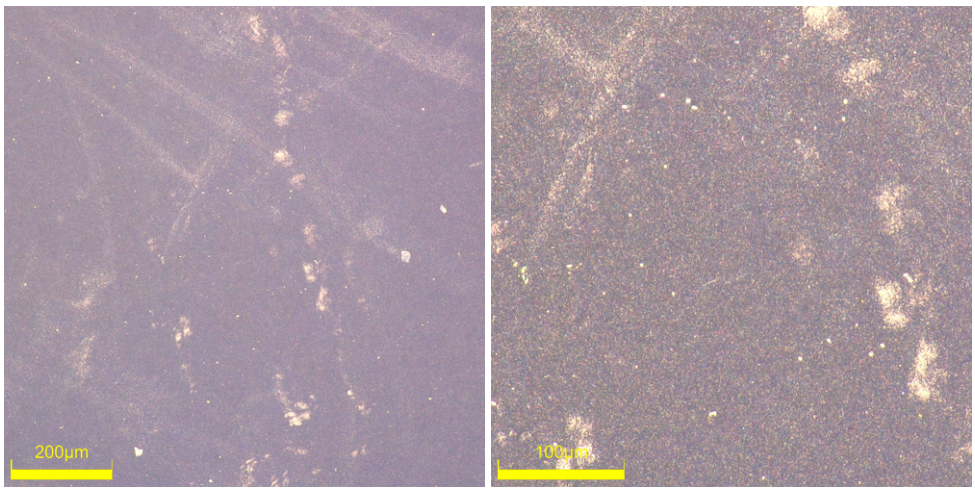

Figure 26 Irradiated graphene mixture with nanotubes surface measured by Olympus digital microscope DSX1000 in brightfield (BF) mode in different scale (200 and 100 μm)

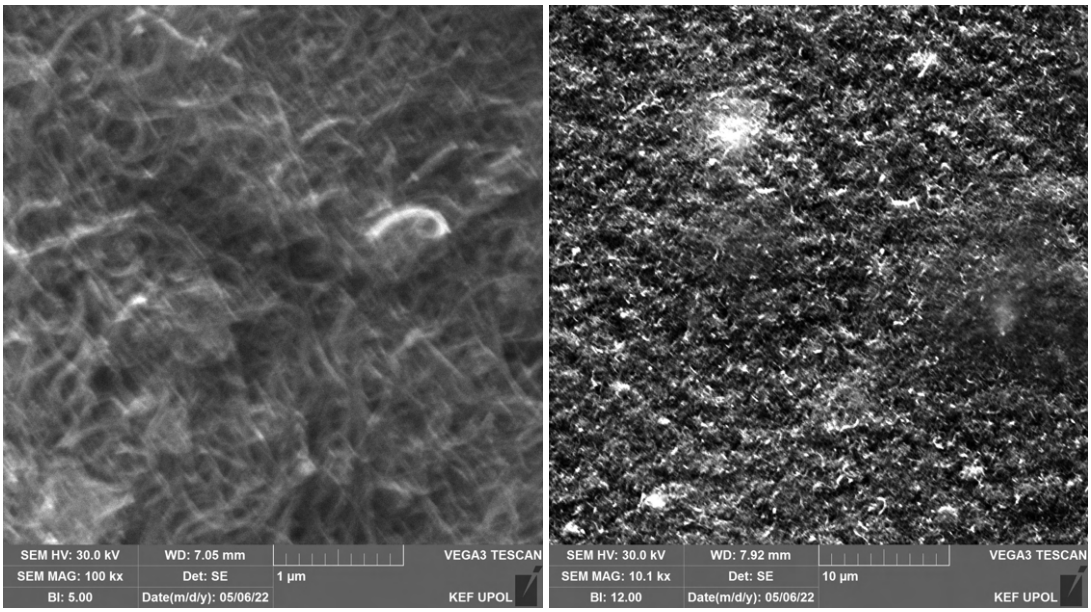

Figure 27 Nonirradiated graphene mixture with nanotubes surface measured by SEM Tescan Vega 3

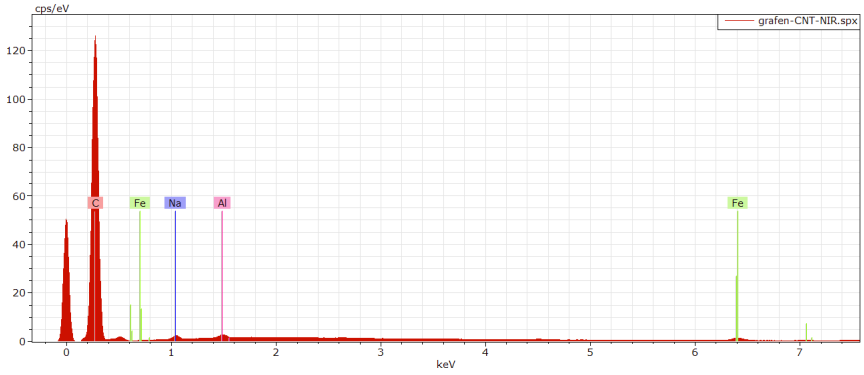

Figure 28 Nonirradiated graphene mixture with nanotubes surface measured by SEM Tescan Vega 3 in EDS mode for elemental mapping

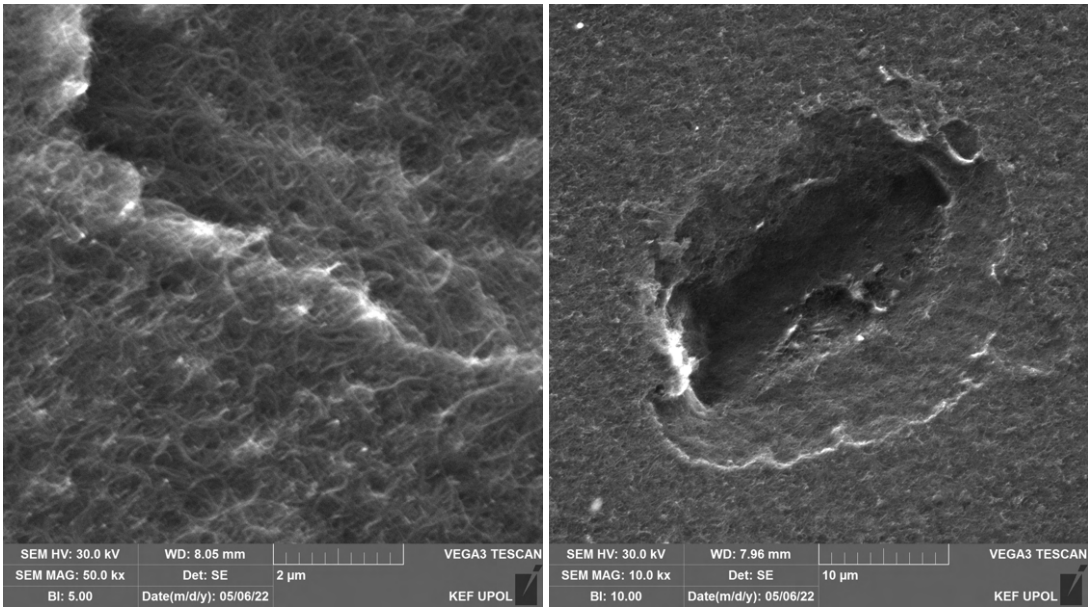

Figure 29 Irradiated graphene mixture with nanotubes surface measured by SEM Tescan Vega 3

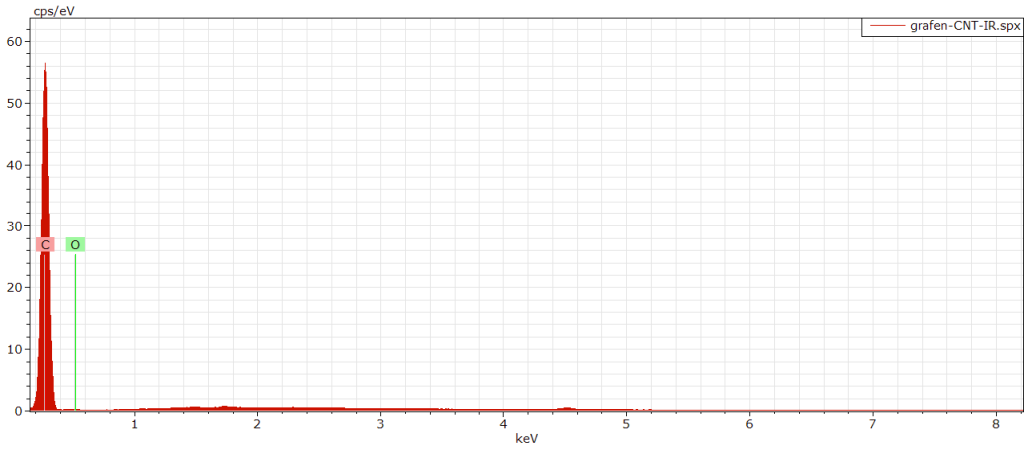

Figure 30 Irradiated graphene mixture with nanotubes surface measured by SEM Tescan Vega 3 in EDS mode for elemental mapping

At fig.25 and at fig.27 we can see the smoth surface of nonirradiated foil fig.23. As we can see, this foil has not any matrix form from another material according to EDS measuring, which is shown at fig.28, where is clear higher purity of carbon element, than at fig.18. It means after irradiation we can not expect changes in elemental mapping as it shown at fig.30. Also we can see at fig.26 and at fig.29 there are no visible surface changes.

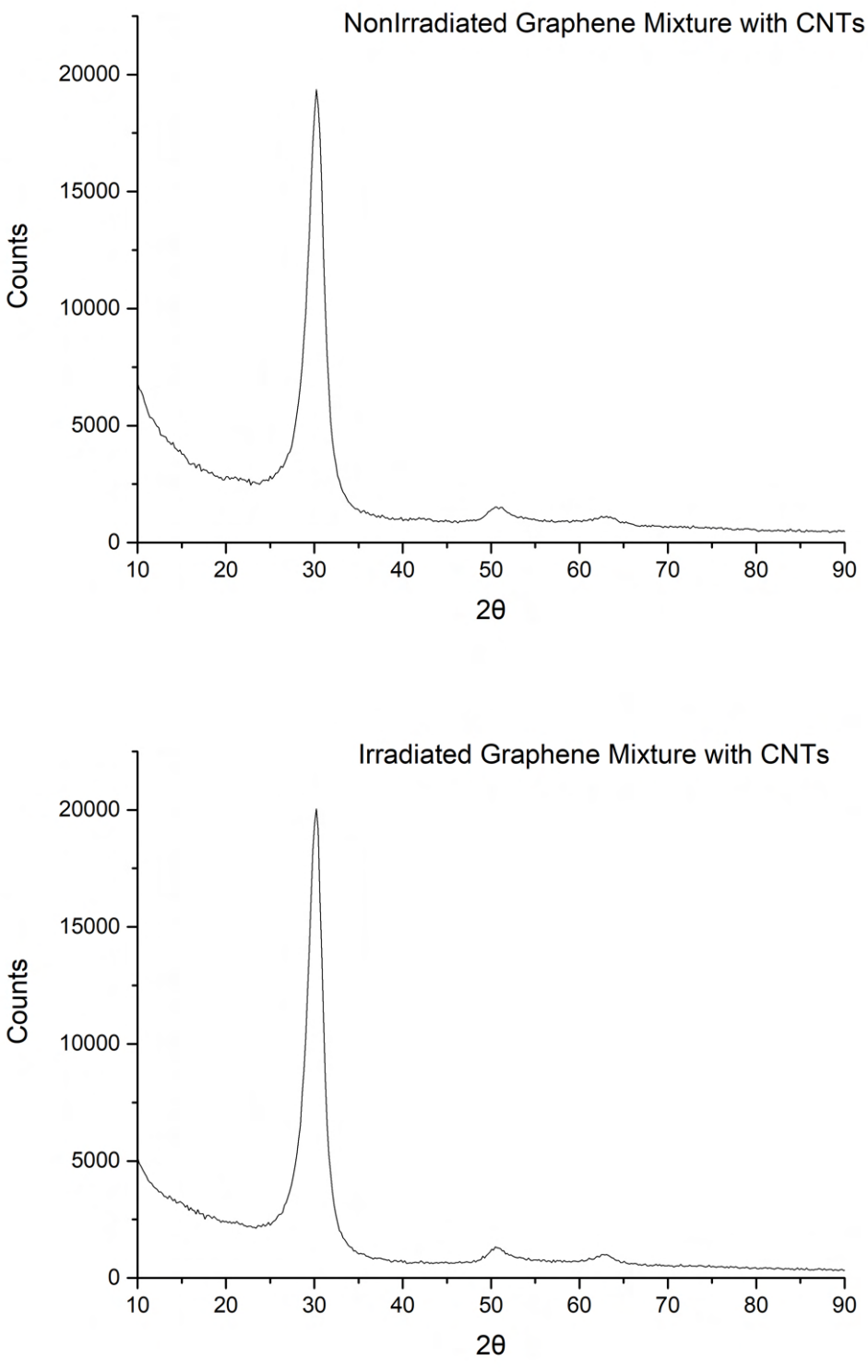

Figure 31 Graphs show us XRD measuring of nonirradiated and irradiated graphene foil with mixture of nanotubes

According to result of XRD (31) and XPS (32) measuring we can not observed any differences between nonirradiated and irradiated graphene foil with mixture of nanotubes, probably it can cause better efficiency as is shown in fig.7.

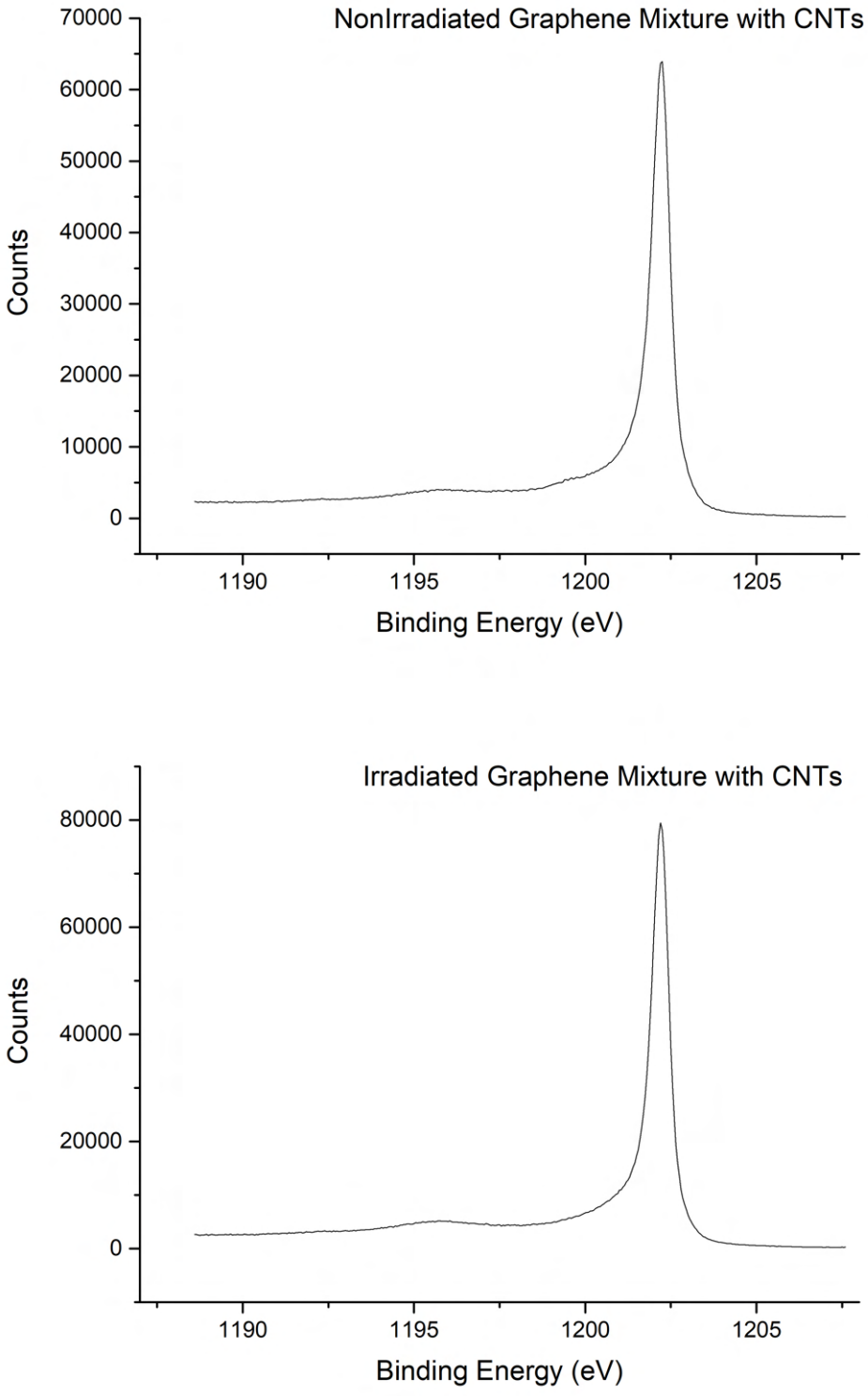

Figure 32 Graphs show us XPS measuring for carbon element of nonirradiated and irradiated graphene foil with mixture of nanotubes

2.5 Foils for degrader of EXP I

In this section were analyzed metal foils from EXP I (1), where alluminium foils at fig.34 and at fig.35 were burned (too thin) and could not be analyzed. With titanium foil marked as Ti No.5 shown at fig.46 was different problem, because in journal (1) was not any mention in data files about changing foils setup to foil at fig.46, but from the fig.33, where is placed in petri dish # 5 AL we can observe significant damage from heat on his surface. Was realized measuring, where irradiated foil was not titanium foil as is wrote in journal (1). The EDS analysis showed, that foil is alluminium. During the experiment could be possible to replace any foils with another. According to this confusion were analyzed foils Al No.3 and Al No.4. Every metal foil before measuring with Olympus digital microscope DSX1000 was cleaned with isopropylalchol, because before was greasy surface.

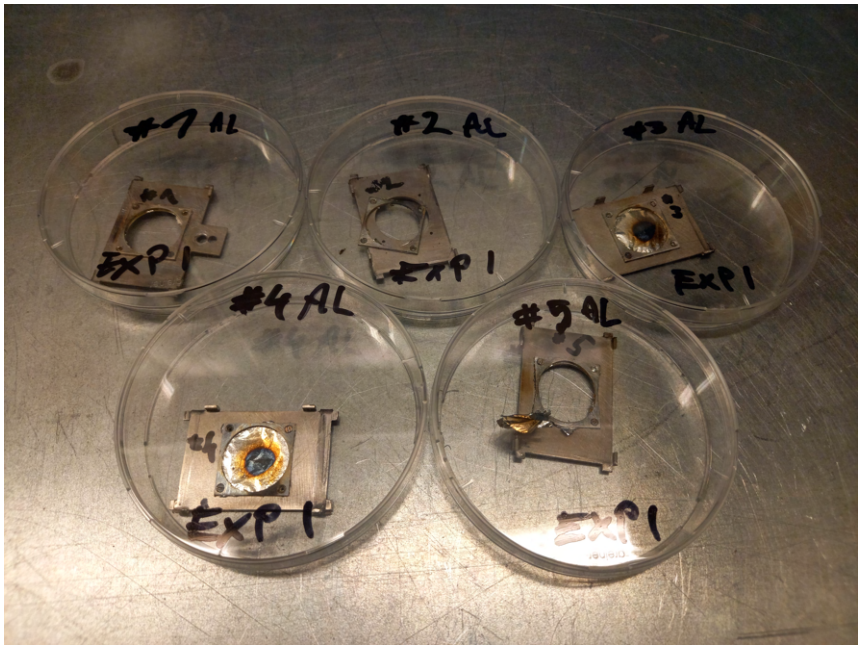

Figure 33 Irradiated metal foils which was taken down from degrader with window holders

2.5.1 Alluminium foil No.1

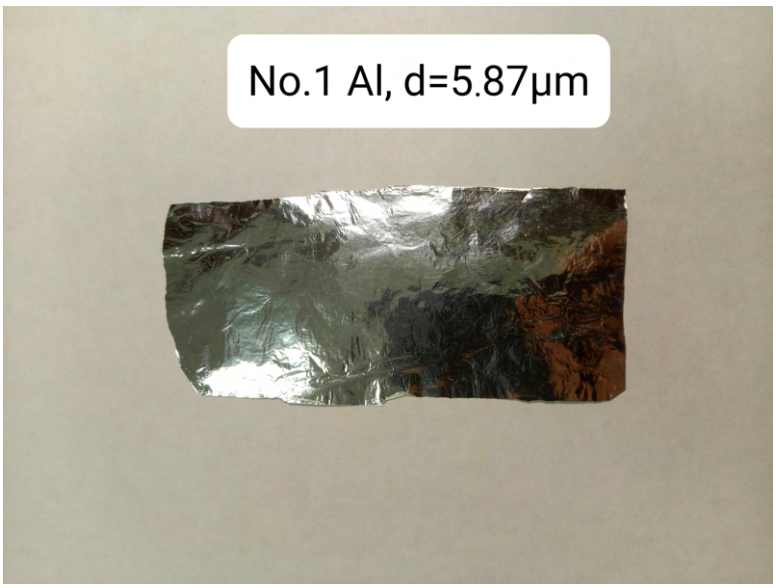

Figure 34 Nonirradiated alluminium foil marked as No.1 with thickness 5.87 μm and with fluence $2.11926 \cdot 10^{17}$ cm^{-2} was used in degrader

2.5.2 Alluminium foil No.2

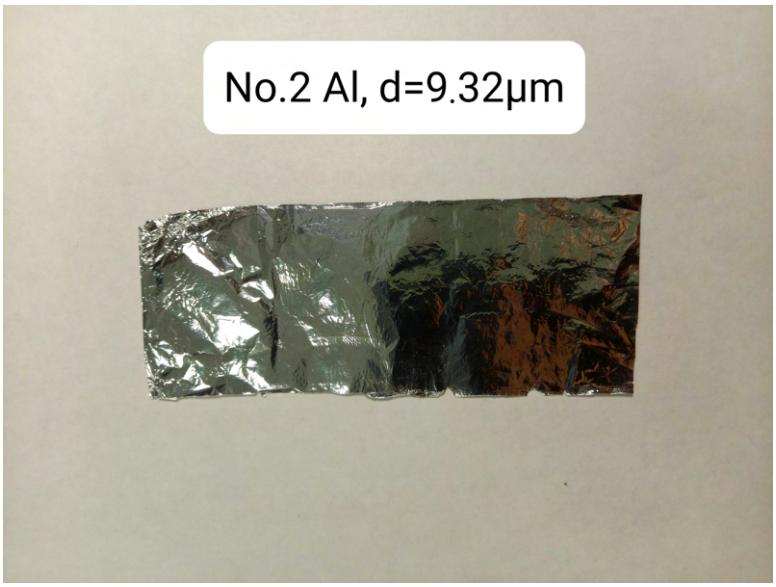

Figure 35 Nonirradiated alluminium foil marked as No.2 with thickness 9.32 μm and with fluence $2.18321 \cdot 10^{17}$ cm^{-2} was used in degrader

The alluminium foils were not been analyzed, because their thickness was to low and were burned during the experiment as we can see at fig.33. It means, that foils are not able for application in degrader.

2.5.3 Alluminium foil No.3

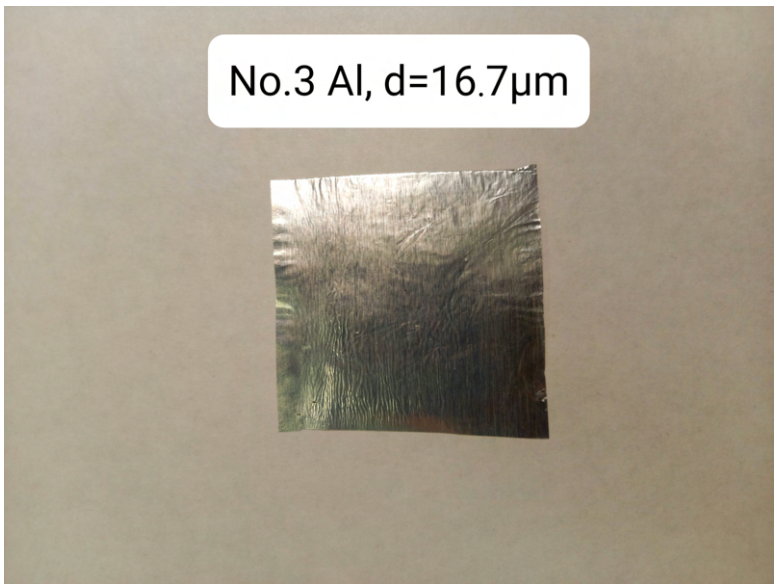

Figure 36 Nonirradiated alluminium foil marked as No.3 with thickness 16.7 μm and with fluence $1.01207 \cdot 10^{17}$ cm^{-2} was used in degrader

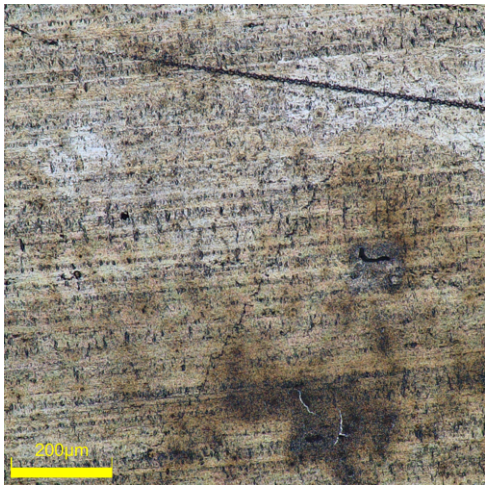

Figure 37 Nonirradiated alluminium foils No.3 surface measured by Olympus digital microscope DSX1000 in brightfield (BF) mode in different scale (200 μm)

At fig.37 of nonirradiated foil from fig.36 we can see the surface with small dent. Low thickness cause manipulation with foils harder. It is really easy to crumple it. After irradiation the foil was not burned, but in the middle of foil was seen heat effect, where the ion beam going through the foil. This irradiated part was analyzed and at fig.38 is possible to see surface changes and heat exposure cause melting on surface. Also at images from SEM at fig.39 we can observe surface changes.

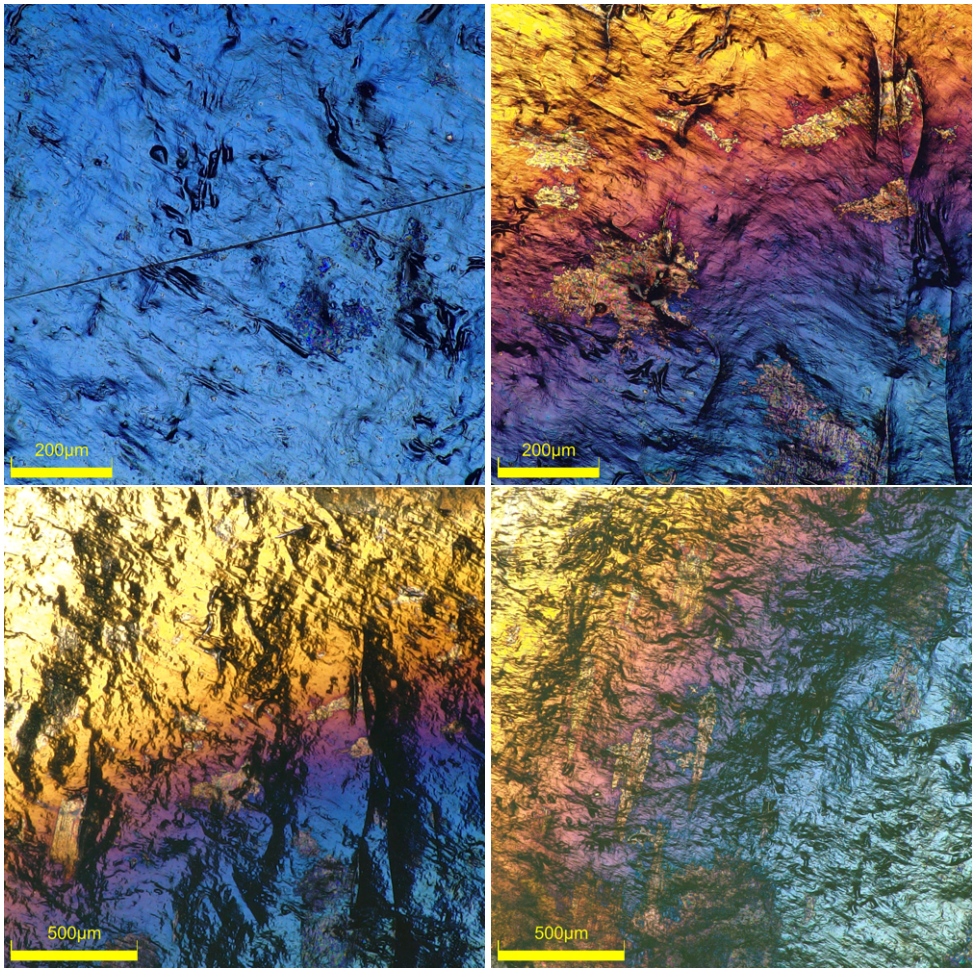

Figure 38 Irradiated alluminium foils No.3 surface measured by Olympus digital microscope DSX1000 in brightfield (BF) mode in different scale (500 and 200 μm)

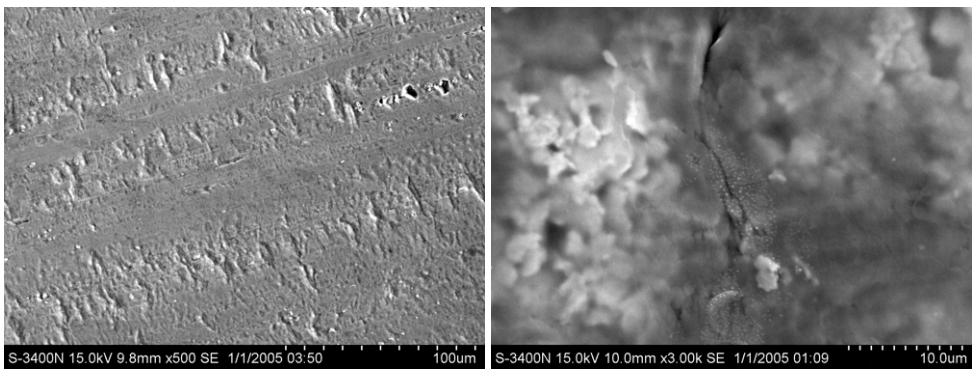

Figure 39 Images of alluminium foils No.3 before and after irradiation measured with SEM Hitachi S-3400 N

At fig.40 from XRD measuring we can observe, that the second peak after irradiation has better signal. It could be cause by irregularities on surface. By XRD software was determined crystallography as COD 4313217, which is defined as cubic crystallography structur according to crystallography open database [16]. At. fig.41 we can see difference between nonirradiated and irradiated foil. According to [17] it could be probably changes from alluminium oxyde to alluminium metal.

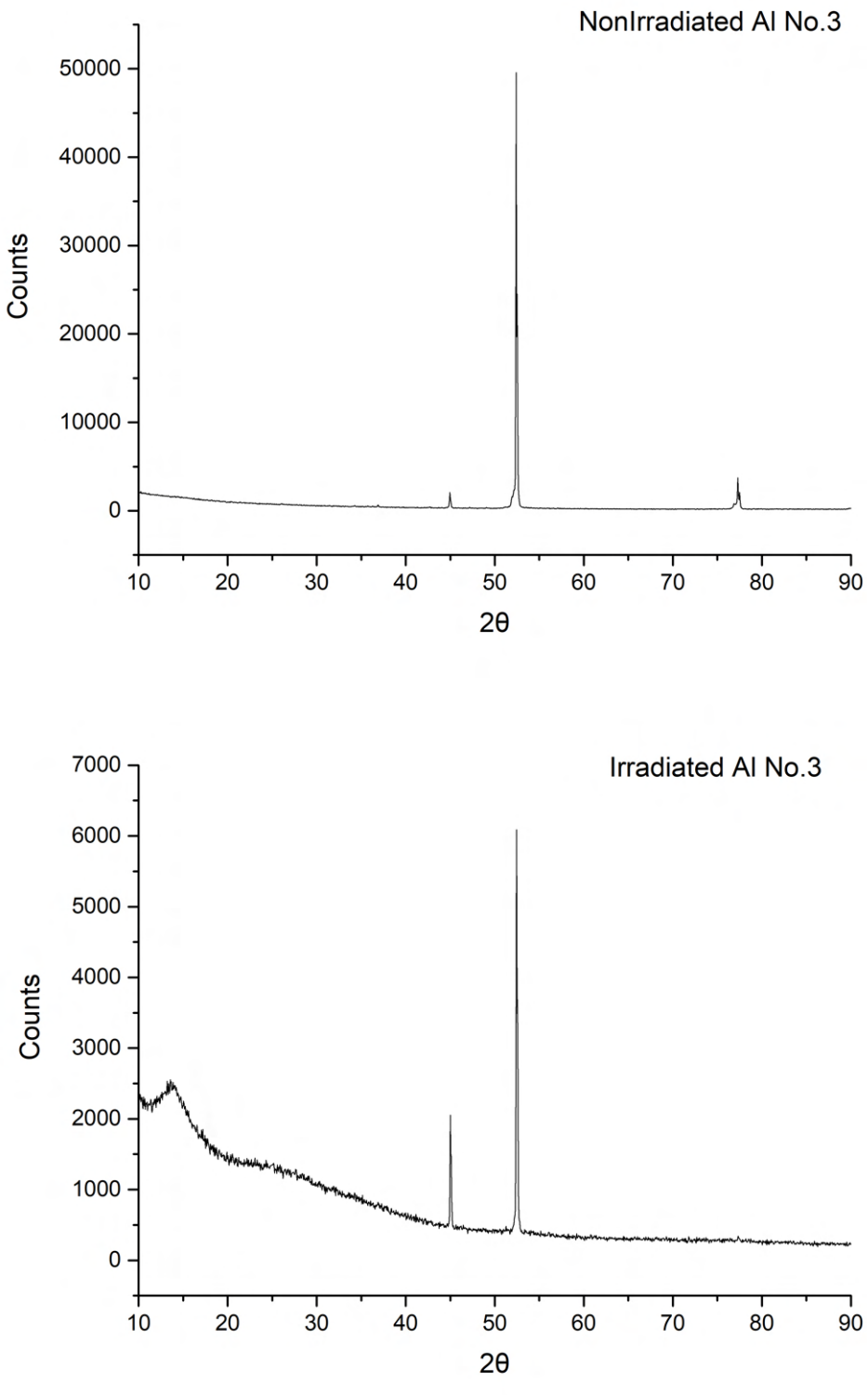

Figure 40 Graphs show us XRD measuring of nonirradiated and irradiated alluminium foil No.3

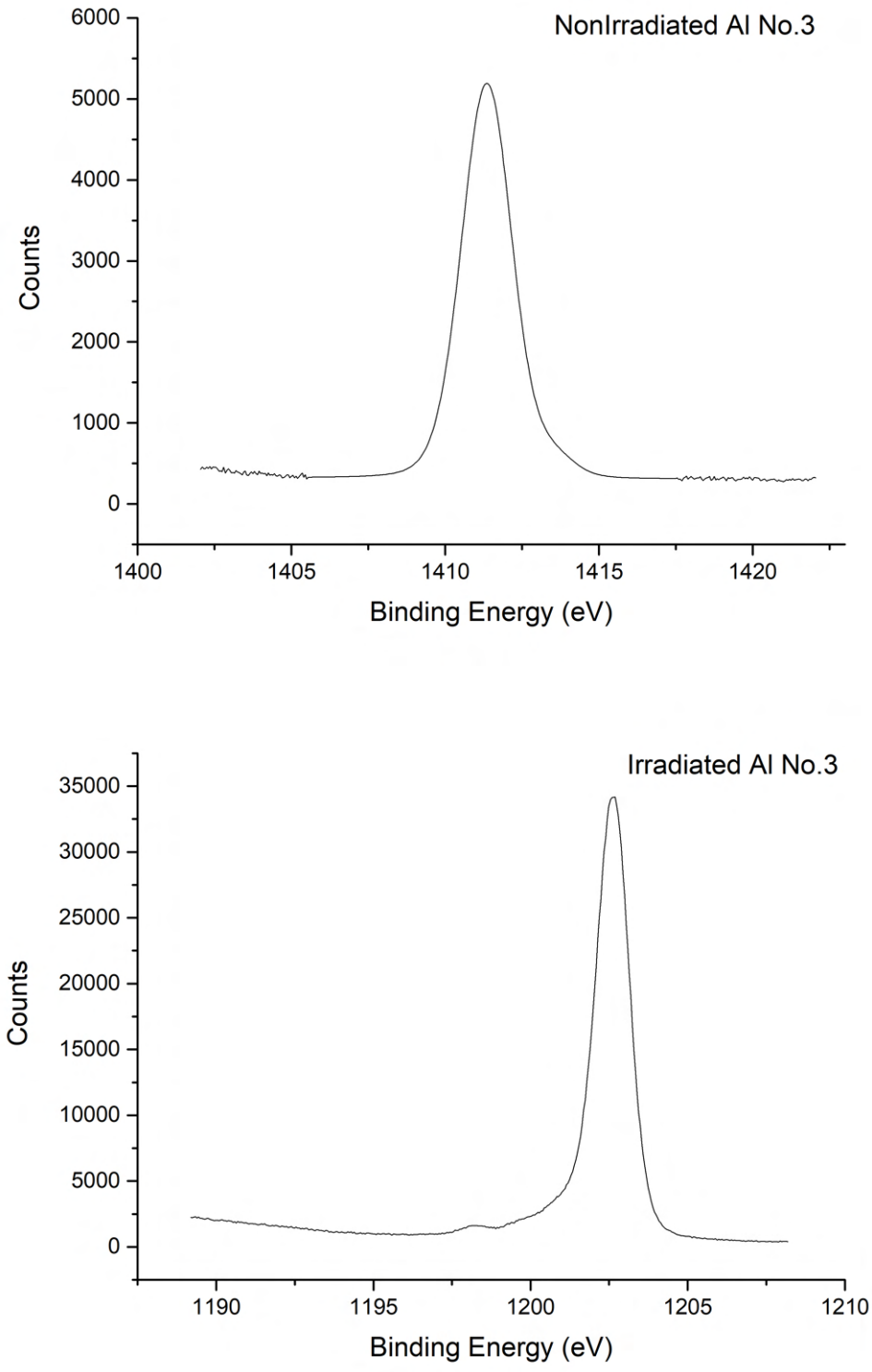

Figure 41 Graphs show us XPS measuring for alluminium element of nonirradiated and irradiated alluminium foil No.3

2.5.4 Alluminium foil No.4

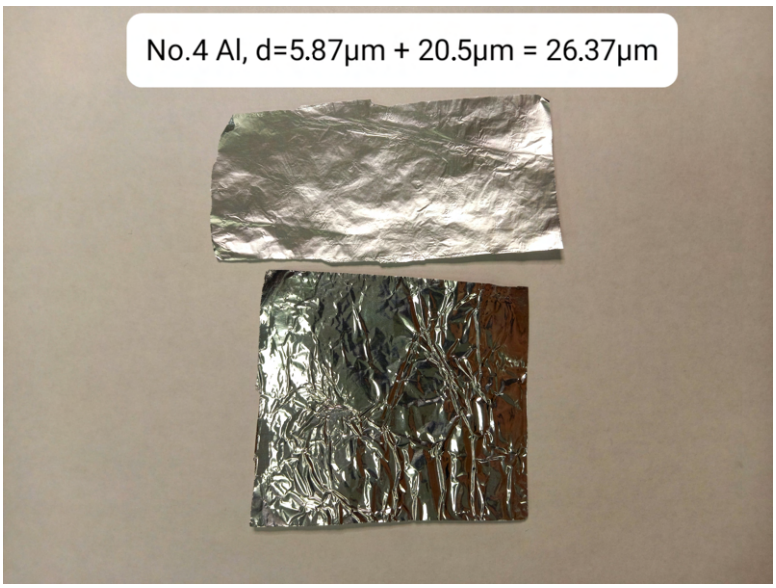

Figure 42 Nonirradiated alluminium foils marked as No.4 with thickness 16.7 μm and with fluence $6.93921 \cdot 10^{16}$ cm^{-2} was used in degrader

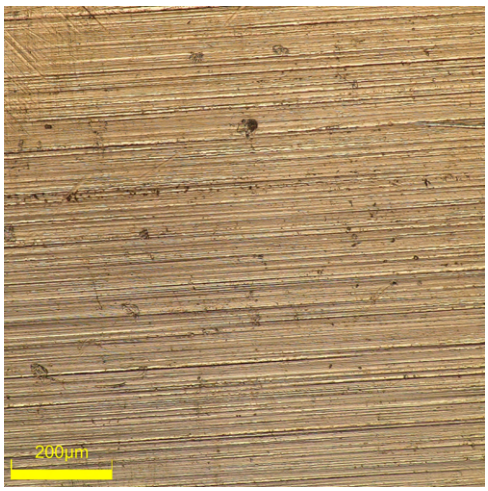

Figure 43 Nonirradiated alluminium foils No.4 surface measured by Olympus digital microscope DSX1000 in brightfield (BF) mode in different scale (200 μm)

Was analyzed one foil from fig.42, because was used only one foil and in journal 1 is not any mention about it. It menas that thickness of analyzed foil is unknown. At fig.43 we can see nonirradiated surface. The surfuce is corrugated from production.

We can see at fig.44 irradiated alluminium foil No.4 from fig.33. It is possible to observe the part of foil, where the ion beam going through the foil, because is charred. The colored stain on the first image is grease and was tried cleaned by isopropyl alcohol. The difference on the surface between fig.43 and fig.44 is big. The irradiated foil changed surface structure and cause heat the surface is melted. At the graphs 45 we can see the peak difference also same as at fig.40 and gained signal from them is really low. The trend of narrowing peak after irradiation is possible to see at every XRD measuring in this theses which could be caused by heat and following cooling.

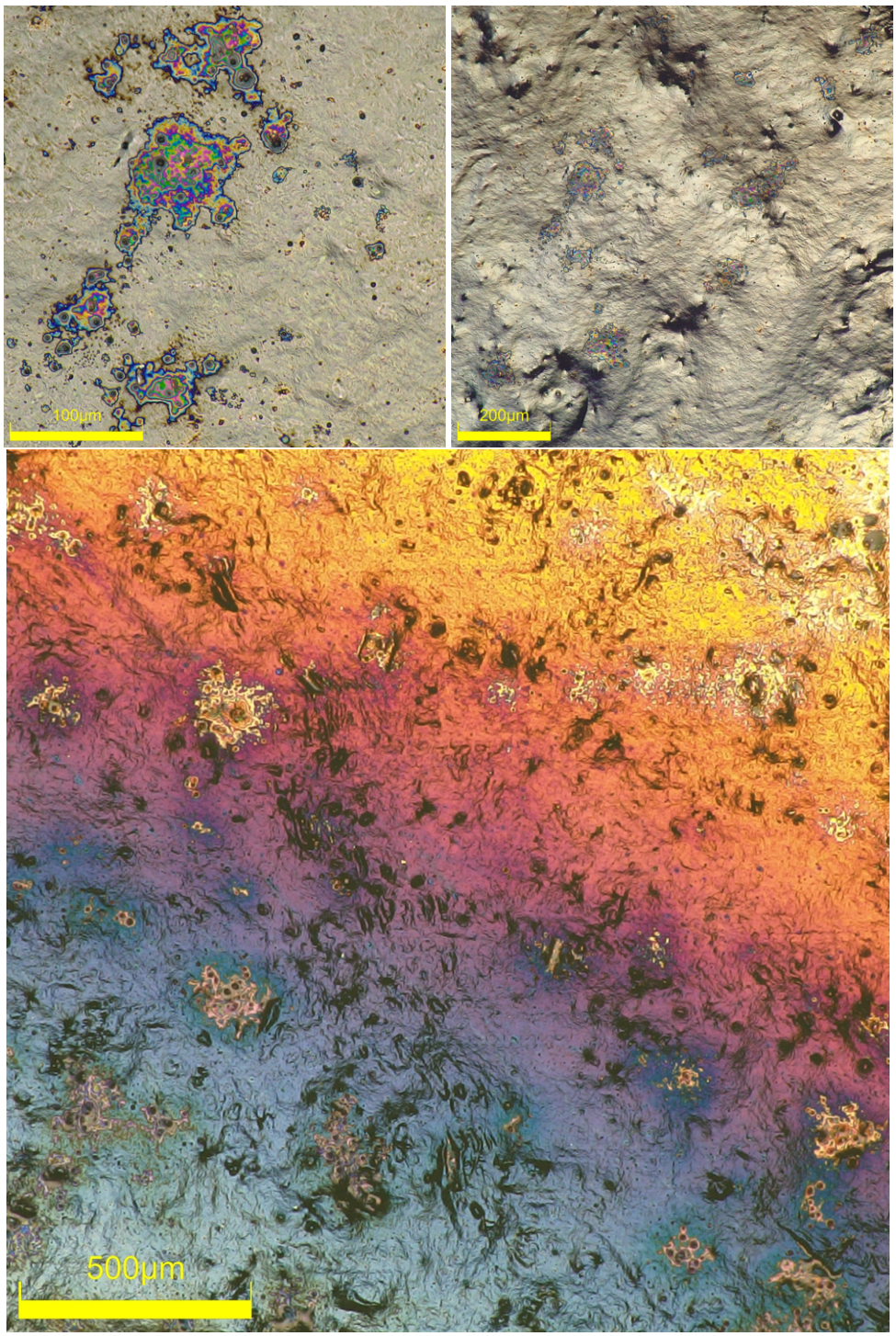

Figure 44 Irradiated alluminium foils No.4 surface measured by Olympus digital microscope DSX1000 in brightfield (BF) mode in different scale (100, 200 and 500 μm)

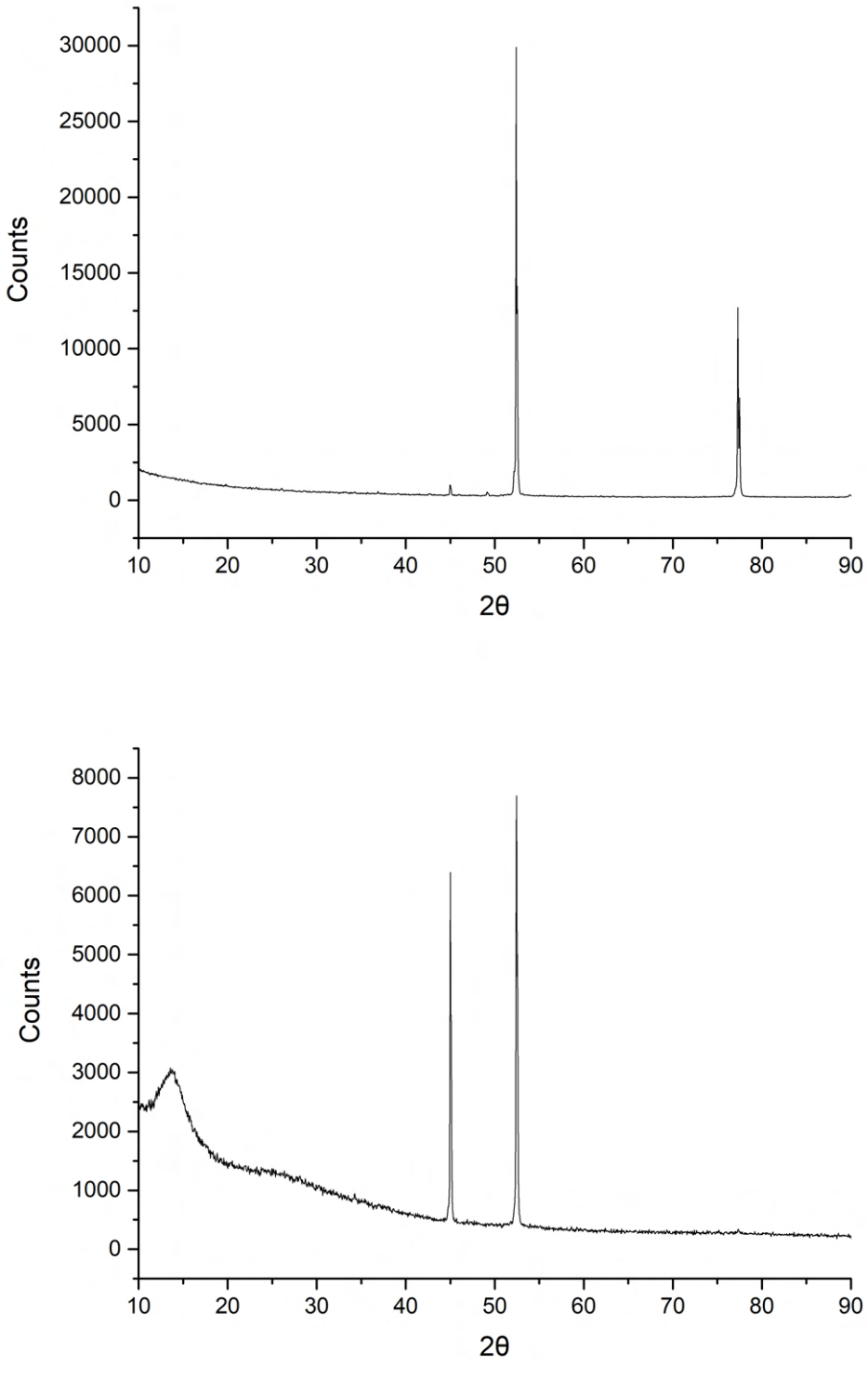

Figure 45 Graphs show us XRD measuring of nonirradiated and irradiated alluminium foil No.4

2.5.5 Titanium foil No.5

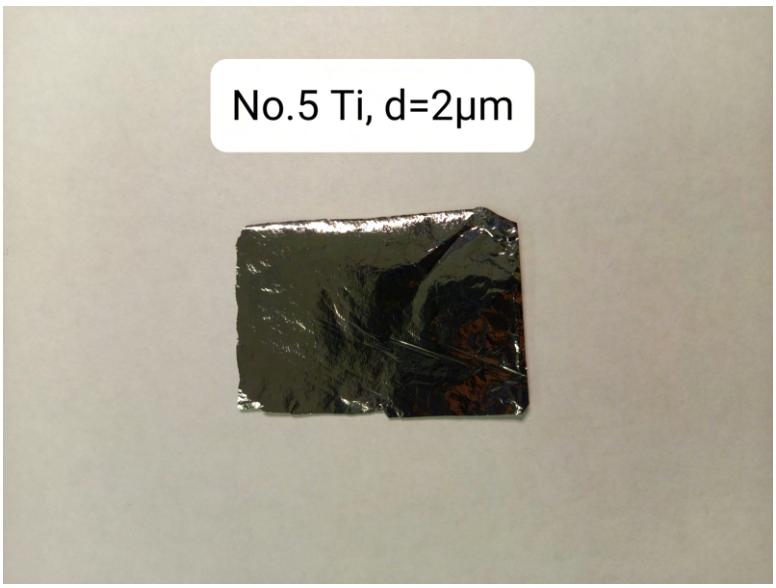

Figure 46 Nonirradiated titanium foils marked as No.5 with thickness 2 μm was used in degrader

The fig.46 was not mention at journal 1, when the setup was changed to foil No.5 not even once. The foil will not be analyzed here, because we do not know anything about it. Were made SEM and EDS analysis and was proven, that the irradiated foil used in EXP I in degrader as foil No.5 was alluminium foil.

2.6 Foils for degrader of EXP II

In second part of the experiment E0919 I analyzed metal foils which was also used as degradation foils. All foils were analyzed, because they are from nickel and titanium and their durabillity of incoming beam is bigger then alluminium foils. Same as in first part, I used same measurment and as I expected also here was made some misstakes. One of the biggest misstake is replacement of irradiation nickel foil see at fig.53 for titanium foil with unknow thickness. Same problem is with titanium foil No.4 see at fig.63, where irradiated foil was not from titanium, but from nickel with unknow thickness. In data files of Exp II nobody mention Titanium foil No.5. see at fig.68 It means, that this foil was obviouslly irradiated see at fig.47, but there are not any note of changing experiment setup to fifth position.

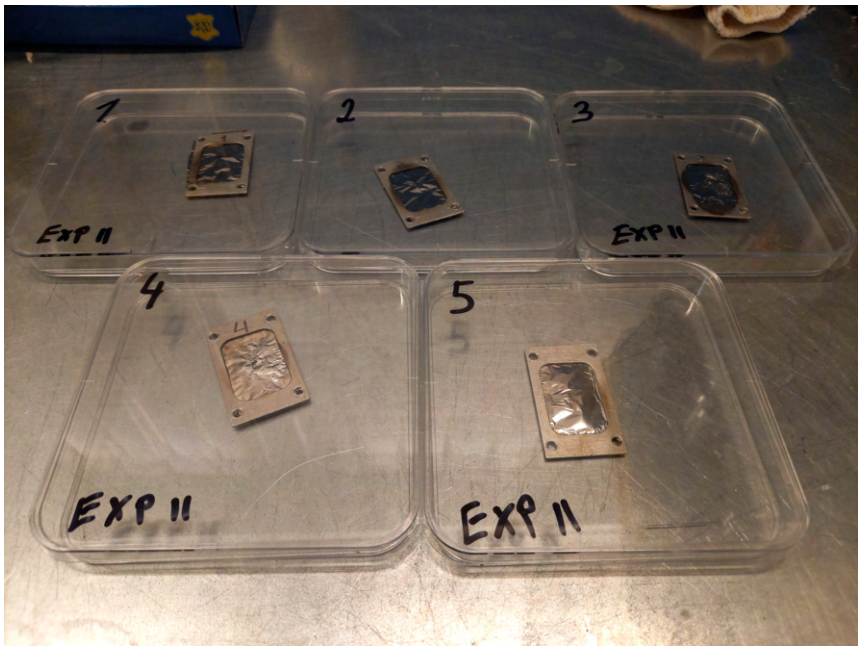

Figure 47 Irradiated metal foils which was taken down from degrader with window holders

2.6.1 Titanium foil No.1

In this section was analyzed titanium foil which was obtained from window holder see at fig.47. In journal 1 was used combination of two titanium foils with diffrent thickness, but at window holder was only one foil. Therefore was analyzed only one titanium foil.

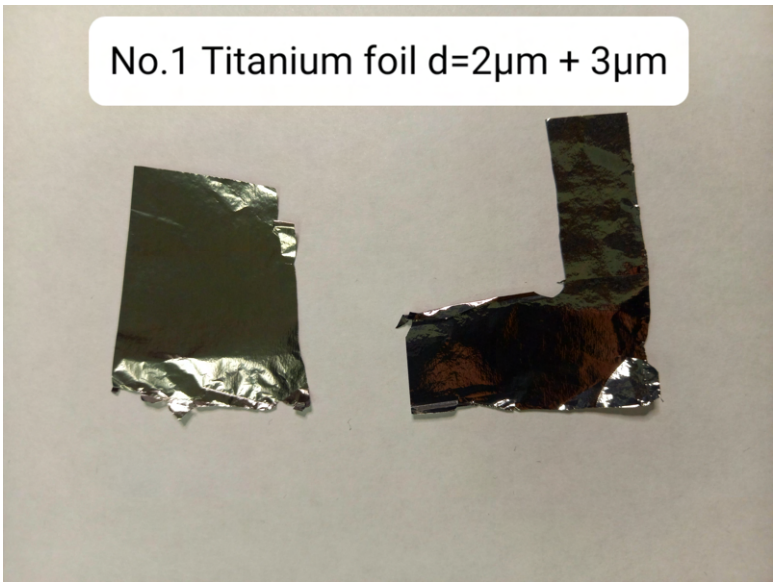

Figure 48 Nonirradiated titanium foils marked as No.1 with thickness 2 μm and 3 μm and with fluence $1.80415 \cdot 10^{16}$ cm^{-2} was used in degrader

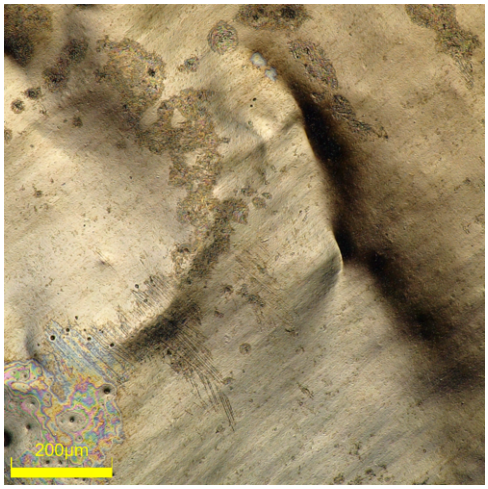

Figure 49 Nonirradiated titanium foils No.1 surface measured by Olympus digital microscope DSX1000 in brightfield (BF) mode in different scale (200 μm)

At fig.49 we can see smooth surface without any damage. It is not perfect flat, because the thickness made it hard for any manipulations. After irradiation see at fig.50, were created on surface small bumps. Durability of this foil during the experiment was without any damage, on the other hand alluminium foils as it see at fig.33 were more damaged. At fig.51 is not see any diffrence before and after irradiation.

After irradiation the peaks grew up and also were created two new peaks. According to XRD software analysis it was determined as cubic crystallography structure with COD 1534878 [19]. Before and after irrabiation the HCP structure was preserved with COD 9016190 according the crystallography open database from [18]

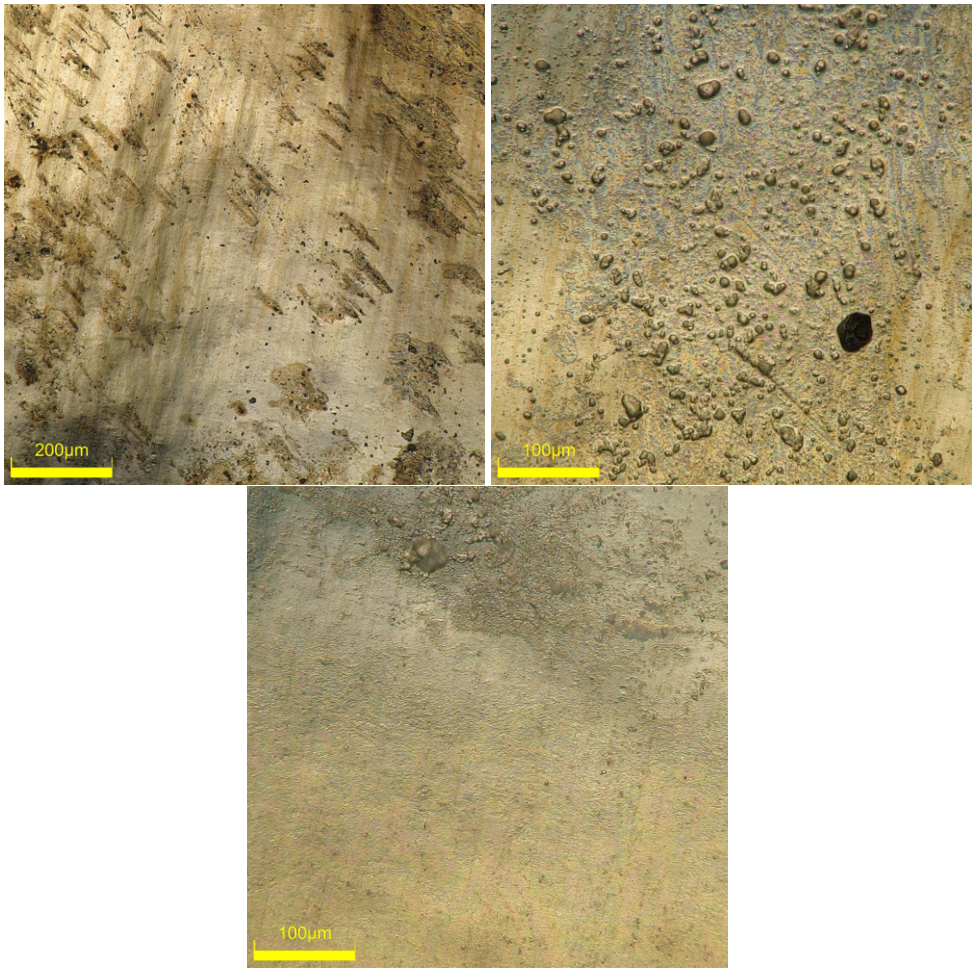

Figure 50 Irradiated titanium foils No.1 surface measured by Olympus digital microscope DSX1000 in brightfield (BF) mode in different scale (200 and 100 μm)

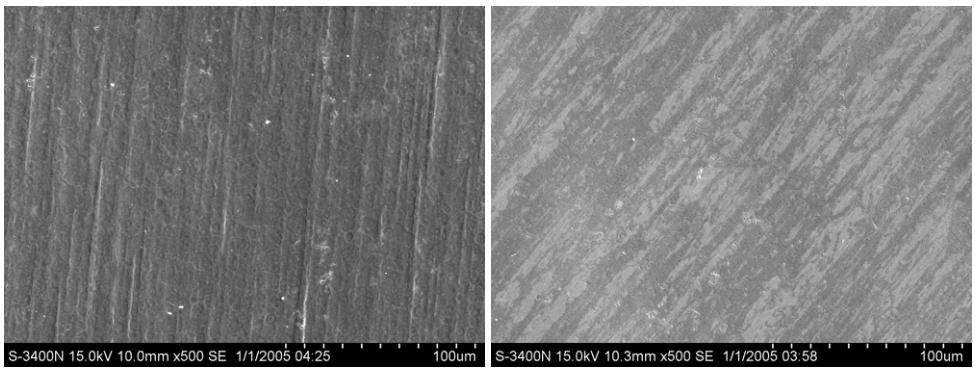

Figure 51 Images of titanium foils before and after irradiation measured with SEM Hitachi S-3400 N

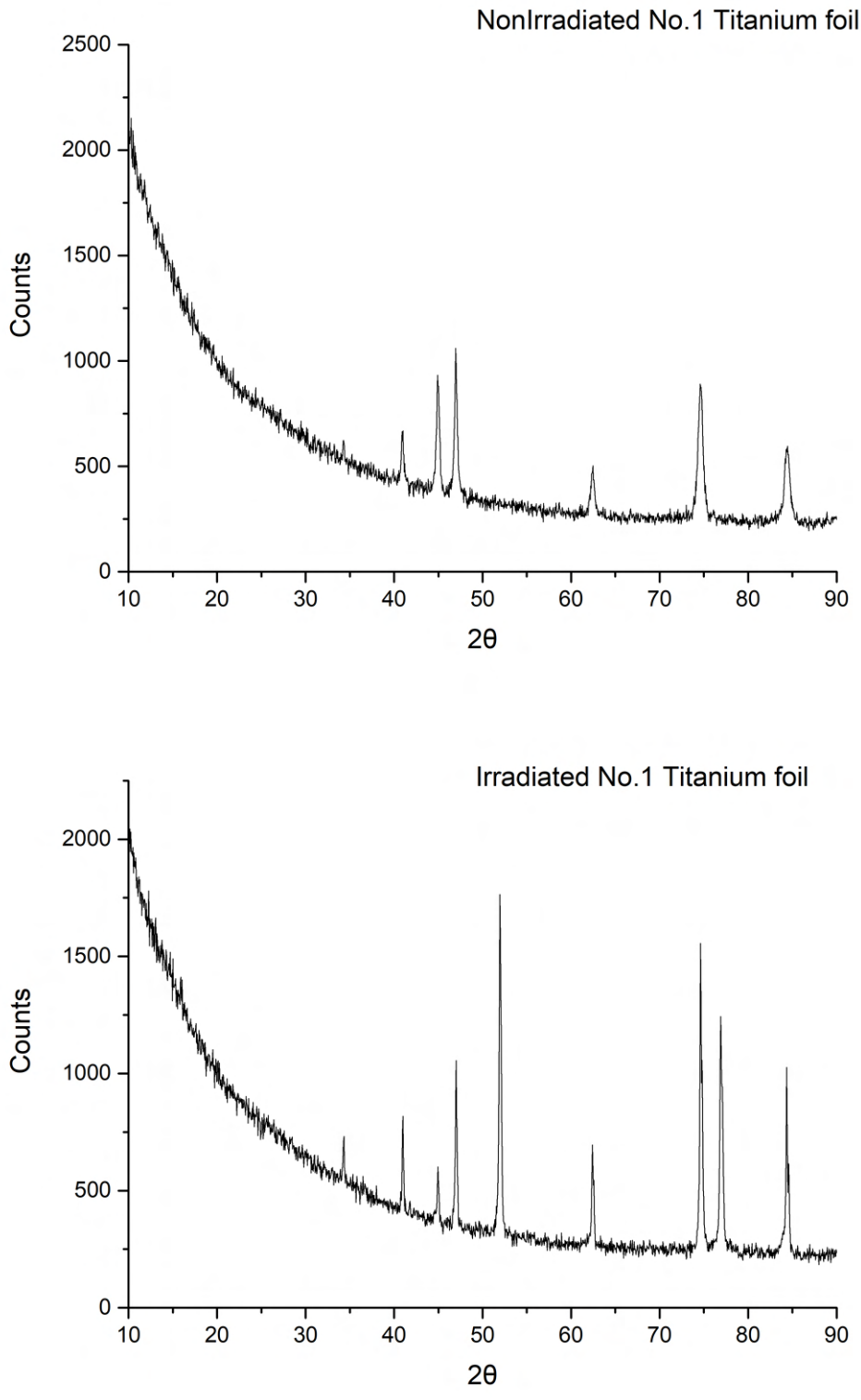

Figure 52 Graphs show us XRD measuring of nonirradiated and irradiated titanium foil No.1

2.6.2 Nickel foil No.2

In this section nonirradiated foil is from nickel and the irradiated foil is from titanium. Were analyzed both of them, but tha data could not be compare, because there are not any information about irradiated foil. Was expected that the foil will be from nickel, but it is not. According to this exchange here would not be data commented except XRD graphs.

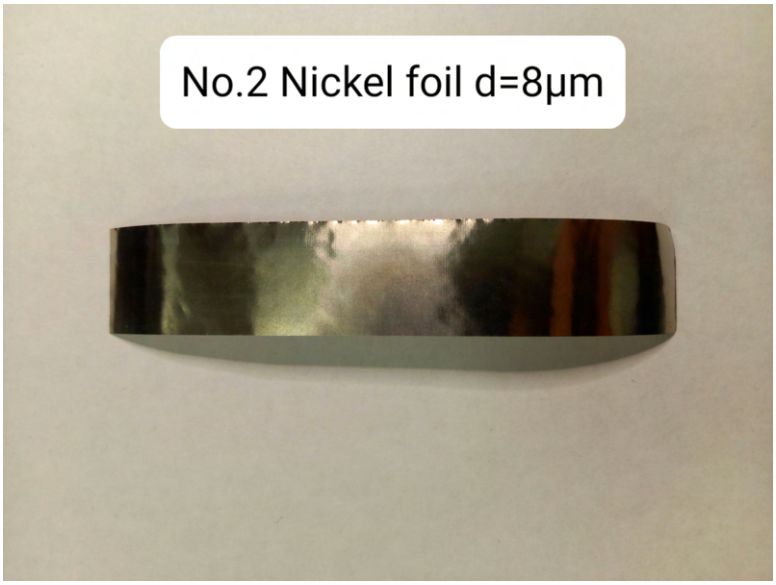

Figure 53 Nonirradiated nickel foils marked as No.2 with thickness 8 μm and with fluence $8.31592 \cdot 10^{15}$ cm^{-2} was used in degrader

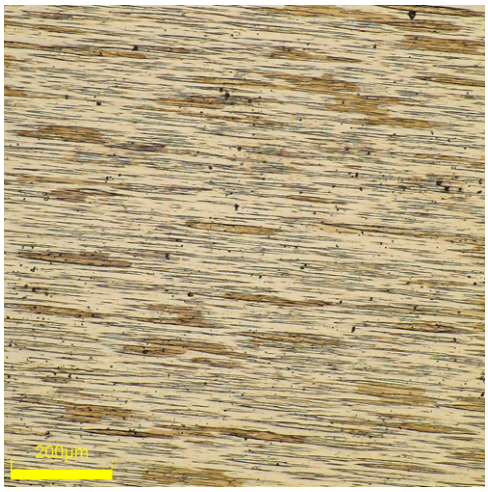

Figure 54 Nonirradiated nickel foils No.2 surface measured by Olympus digital microscope DSX1000 in brightfield (BF) mode in different scale (200 μm)

The spectrums from XRD see at fig.57 are different, it is because they are two different materials. Nonirradiated from nickel a irradiated from titanium. For nickel XRD software determined a COD 4320489 according to [20] which is cubic crystal structure. On the other hand irradiated titanium foil No.2 was determined a COD 9008517 by XRD software, which is HCP crystal structure according to [21]. If the irradiated foil is same foil, which was used same as here 2.6.1, is possible to observe similar peaks of nonirradiated titanium foil see at fig.52.

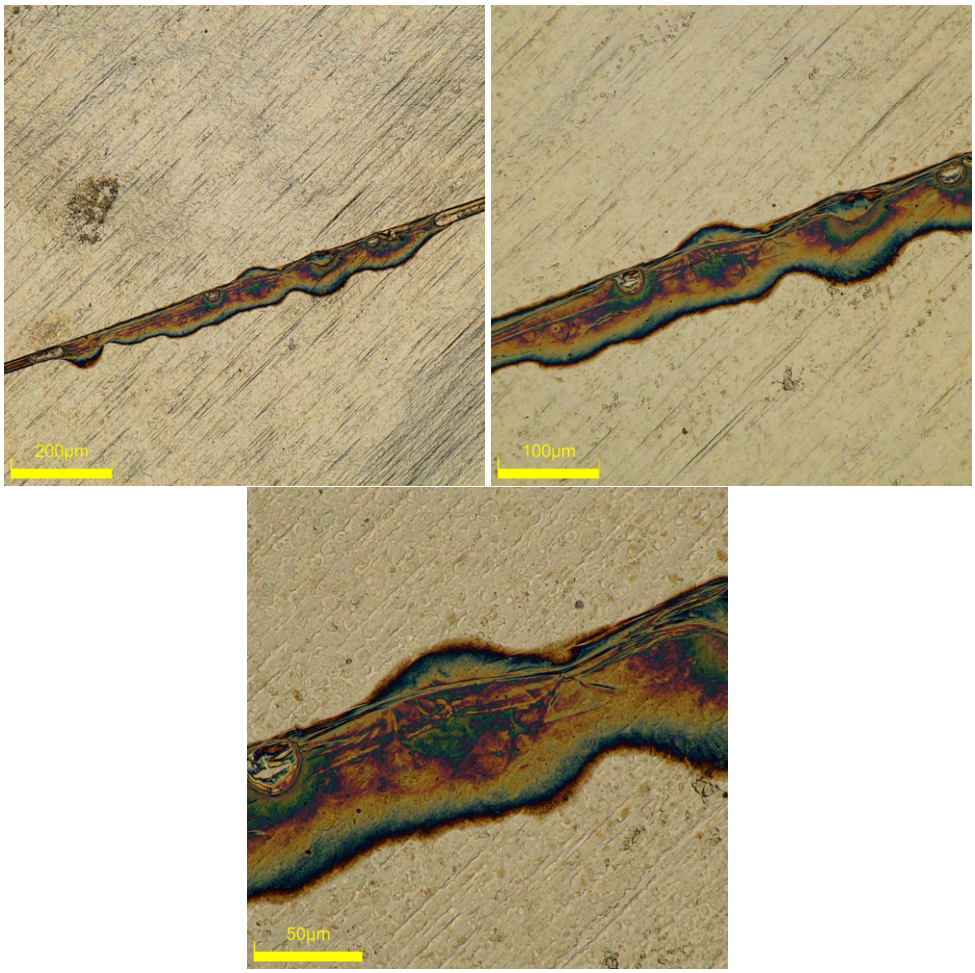

Figure 55 Irradiated titanium foils No.2 surface measured by Olympus digital microscope DSX1000 in brightfield (BF) mode in different scale (200, 100 and 50 μm)

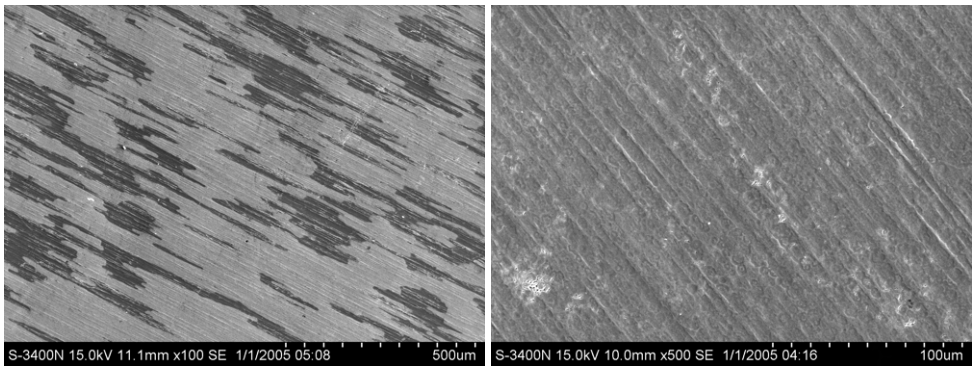

Figure 56 Images of nickel foil No.2 before irradiation and titanium foil No.2 after irradiation measured with SEM Hitachi S-3400 N

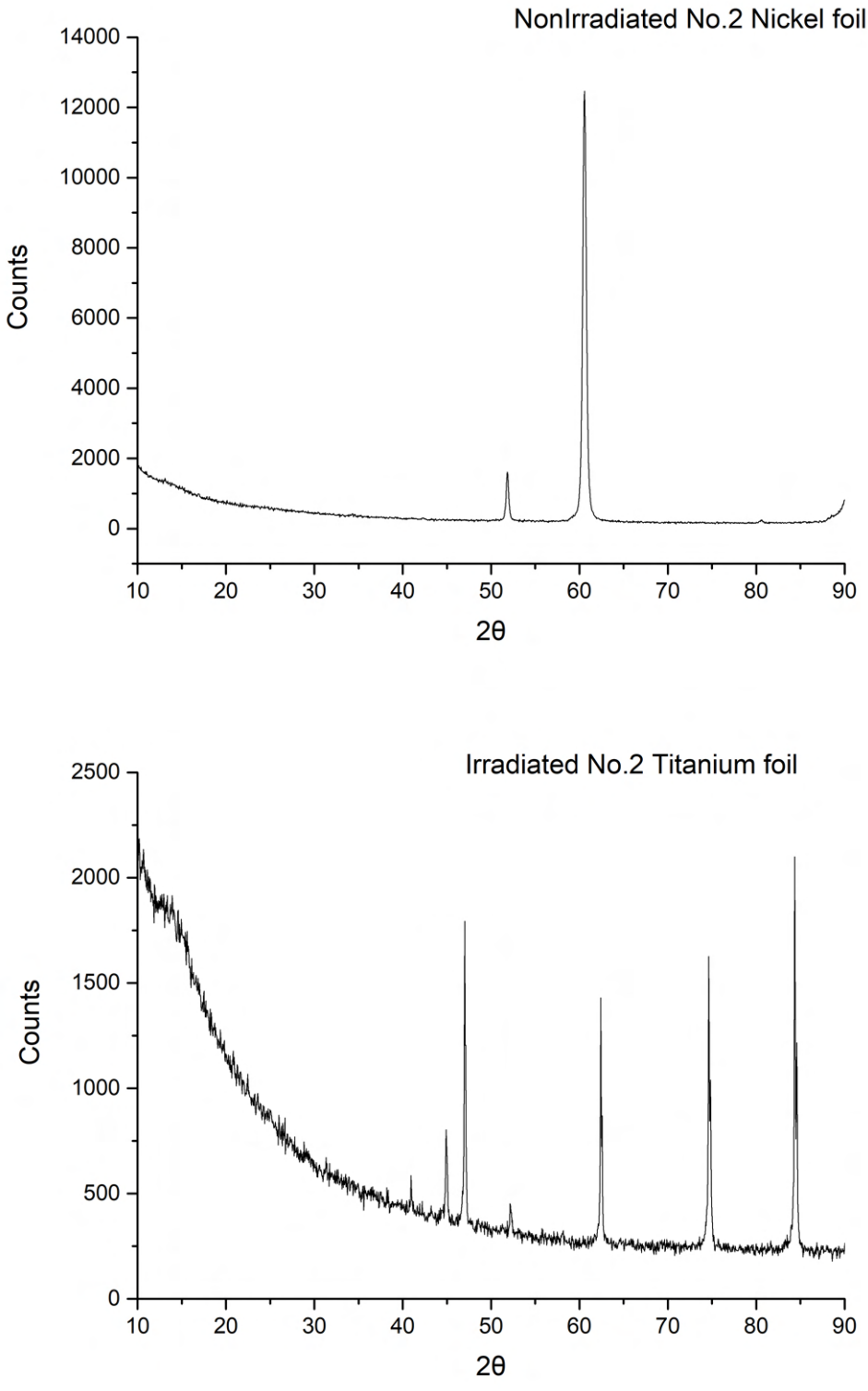

Figure 57 Graphs show us XRD measuring of nonirradiated nickel foil No.2 and irradiated titanium foil No.2

2.6.3 Nickel foil No.3

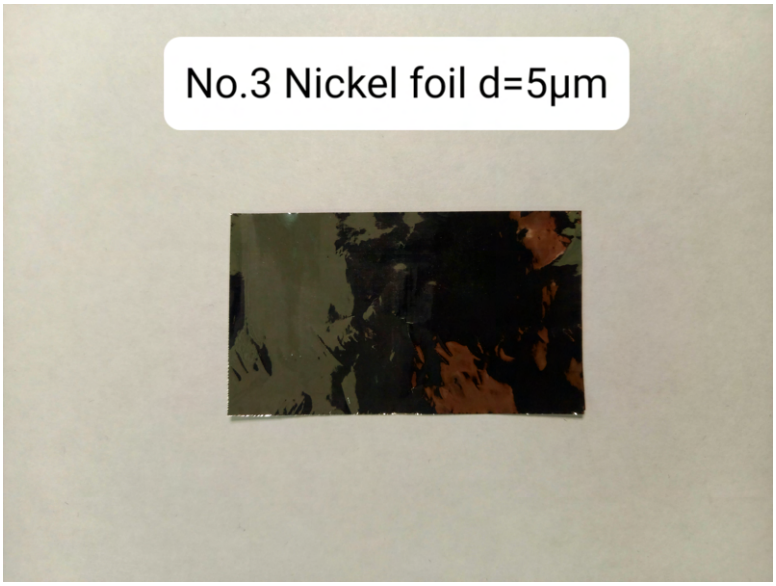

Figure 58 Nonirradiated nickel foils marked as No.3 with thickness 5 μm and with fluence $2.486 \cdot 10^{16}$ cm^{-2} was used in degrader

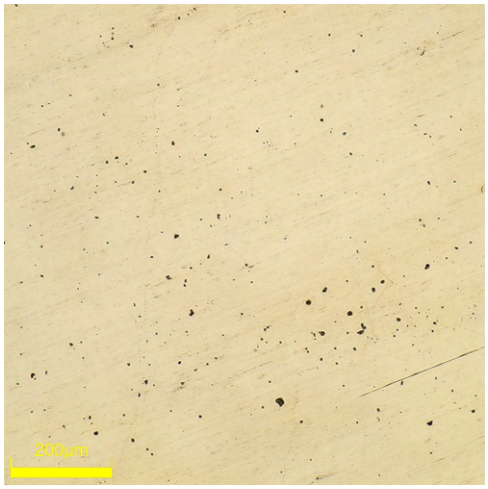

Figure 59 Nonirradiated nickel foils No.3 surface measured by Olympus digital microscope DSX1000 in brightfield (BF) mode in different scale (200 μm)

At fig.58 is reference foil, which was obtained from members of MASHA group. At fig.59 is the surface of nonirradiated nickel foil No.2 and it is relatively clean. After irradiation see at fig.60 the surface was changed. At the second image of fig.60 is melted part on the surface.

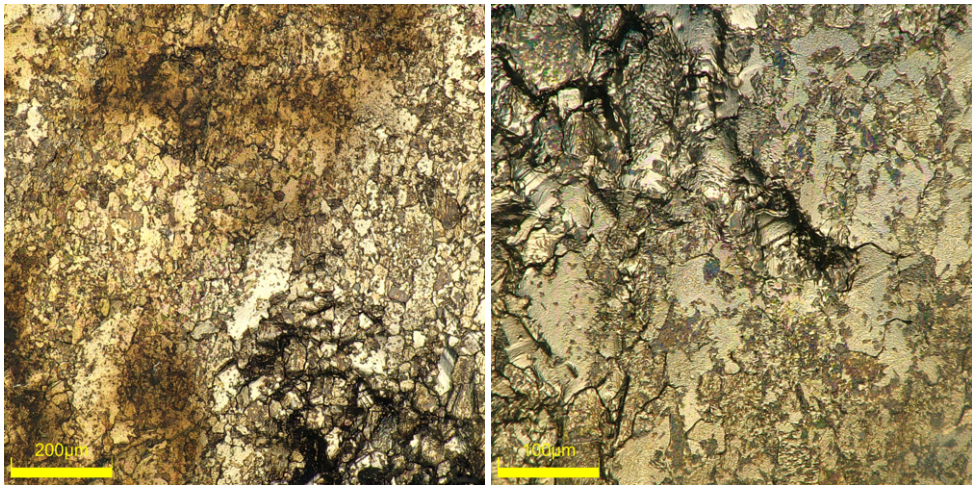

Figure 60 Irradiated nickel foils No.3 surface measured by Olympus digital microscope DSX1000 in brightfield (BF) mode in different scale (200 and 100 μm)

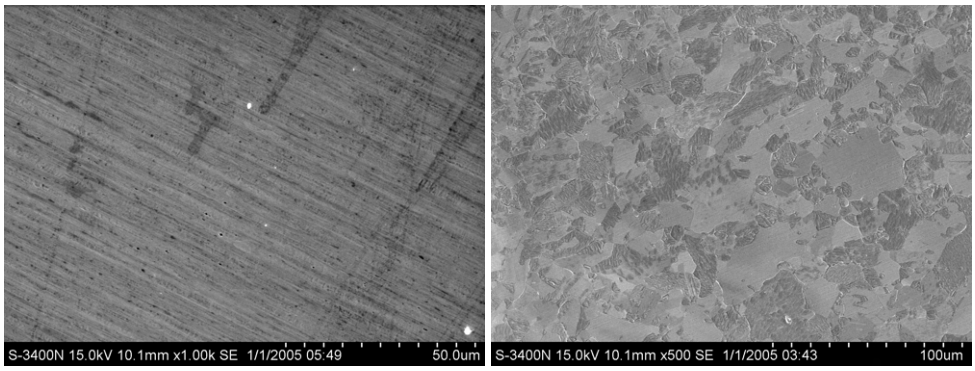

Figure 61 Images of nickel foil No.3 before irradiation and after irradiation measured with SEM Hitachi S-3400 N

At fig.61 first image is nonirradiated nickel foil No.2 and the second one is irradiated. The surface change is visible. Is not smooth without damage and also not homogenous. The spectrums from XRD measuring see at fig.62 show us, that there is no crystal structure change. Same as for nonirradiated nickel No.2 53 was determined same COD 4320489 by XRD software according to [20], which is cubic crystal structure.

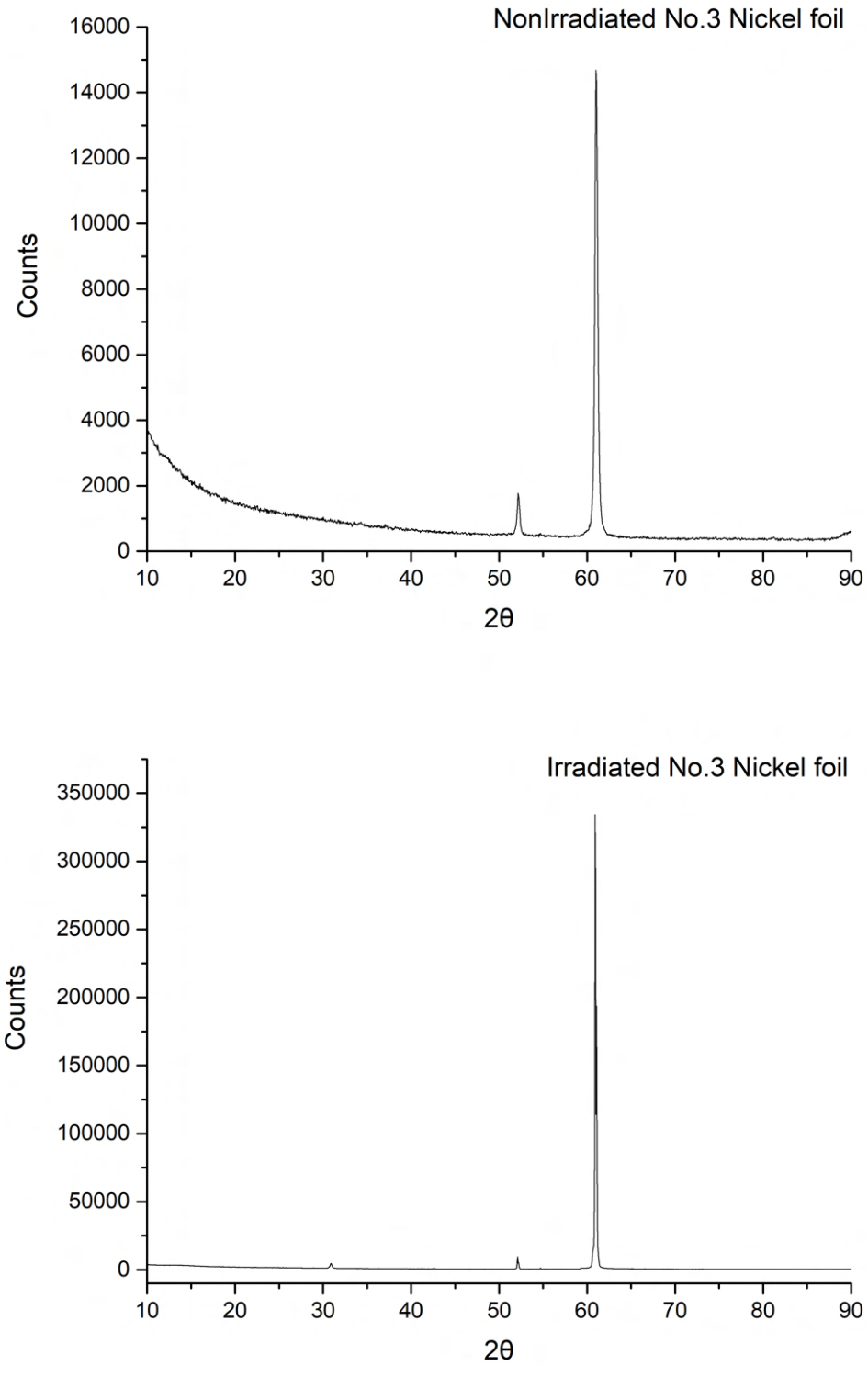

Figure 62 | Graphs show us XRD measuring of nonirradiated nickel foil No.3

2.6.4 Titan foil No.4

Similar problem happened at 2.6.2, happened here, but here was exchanged titanium foil for nickel foil with unknown information, without anymention.

Figure 63 Nonirradiated titanium foils marked as No.4 with thickness 3 μm and with fluence $6.06879 \cdot 10^{15}$ cm^{-2} was used in degrader

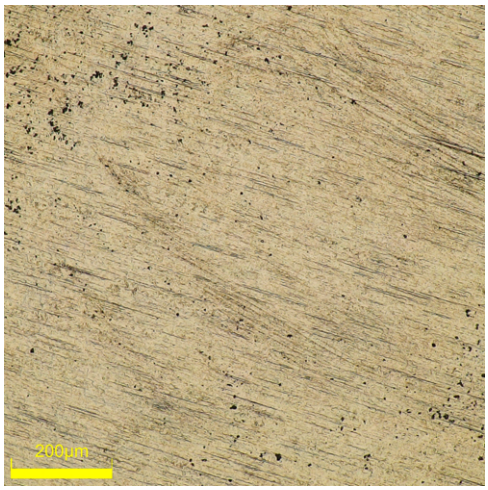

Figure 64 Nonirradiated titanium foils No.4 surface measured by Olympus digital microscope DSX1000 in brightfield (BF) mode in different scale (200 μm)

Titanium foil at fig.63 was obtained from members of MASHA group. At fig64 is nonirradiated surface of titanium foil, where we can not see any crumled. At fig.65 is possible to see surface of irradiated nickel foil, which is very similar to fig.60. Because one measuring of nonirradiated titanium and nickel was done before, at fig.66 is only irradiated nickel foil No.4, where is possible to see different roughness of surface.

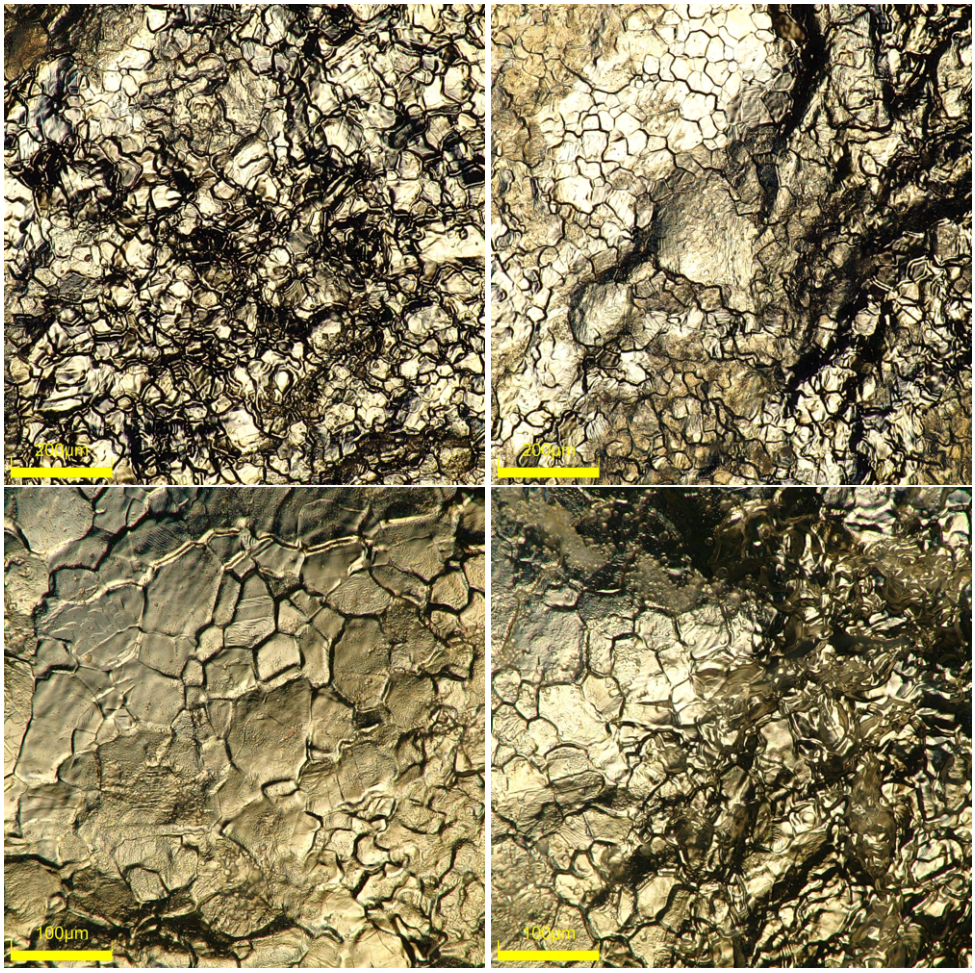

Figure 65 | Irradiated nickel foils No.4 surface measured by Olympus digital microscope DSX1000 in brightfield (BF) mode in different scale (200 and 100 μm)

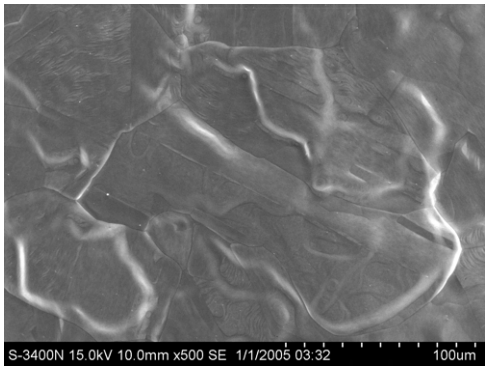

Figure 66 | Images of nickel irradiated foil No.4 measured with SEM Hitachi S-3400 N

At fig.67 are two spectrums from XRD measuring, where the difference between them is large. It means, that there are two foil from different material. XRD software determined nonirradited as titanium foil with COD 9008517 according to [21], which is HCP crystal structure. On the other hand the irradiated foil was determined as nickel with COD 4320498 according to [20], which is cubic crystal structure. The bigger signal for first peak could be caused by the roughness of suface.

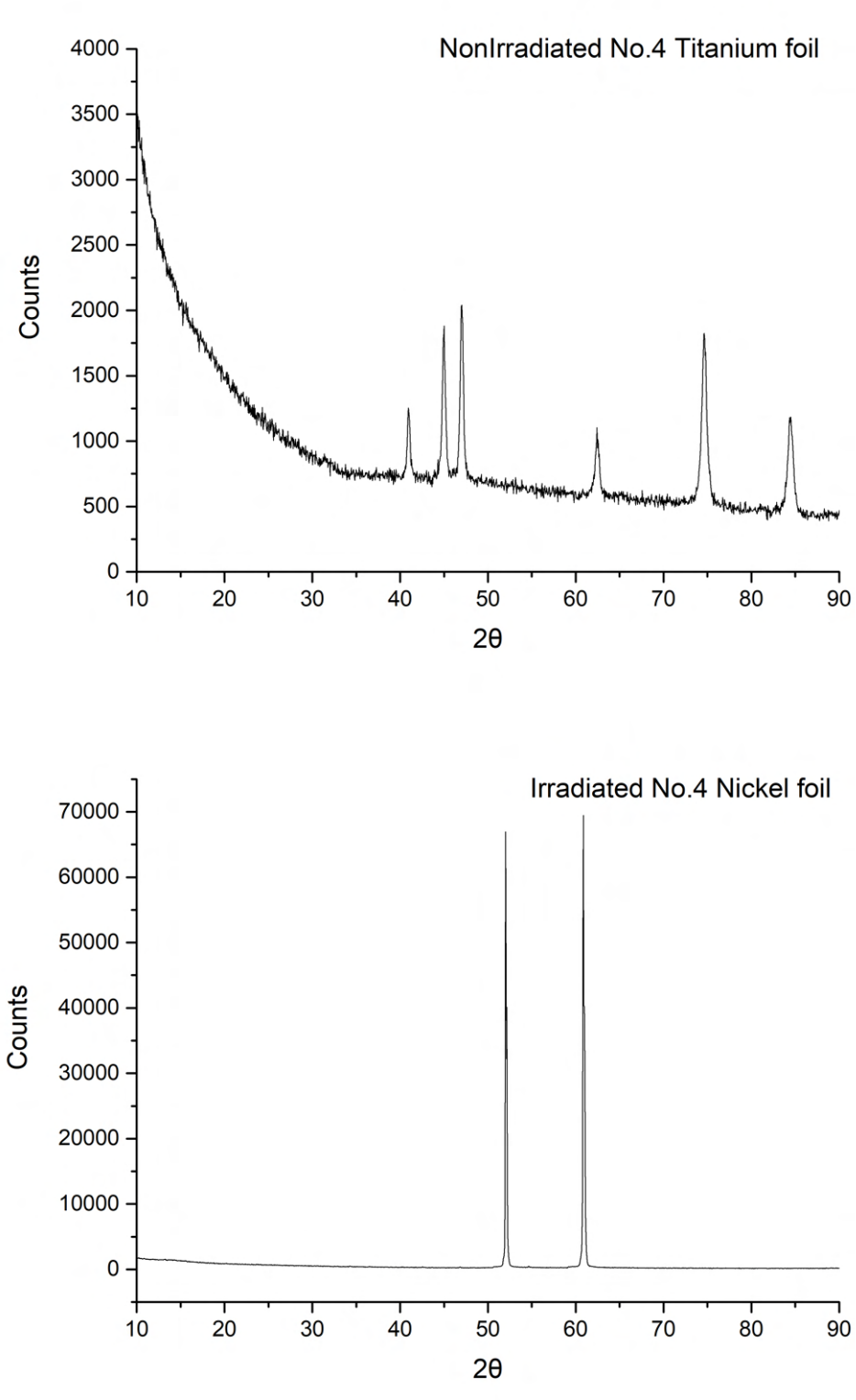

Figure 67 Graphs show us XRD measuring of nonirradiated titanium foil No.4 and irradiated nickel foil No.4

2.6.5 Titan foil No.5

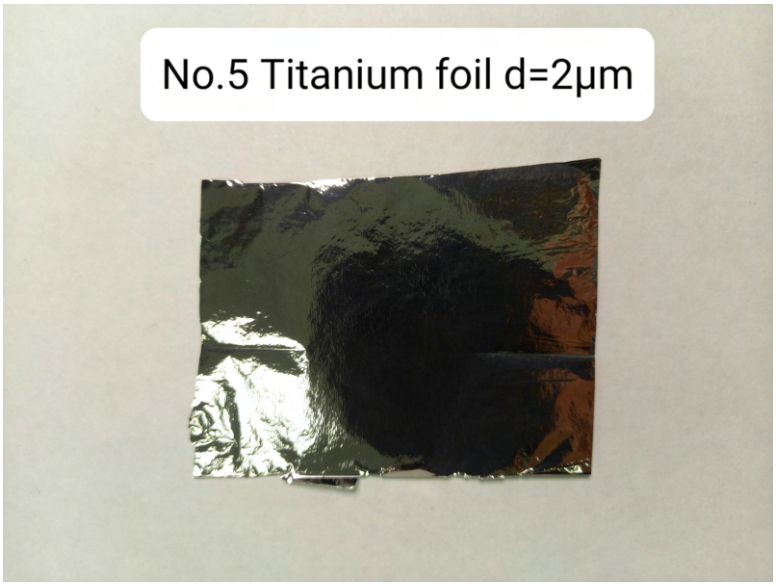

Figure 68 | Nonirradiated titanium foils marked as No.5 with thickness 2 μm

This foil see at fig.68 was obtained from members of MASHA group. This foil was not mention at journal 1. According to fig.47 the fifth foil was irradiated, it means was used during the experiment, but this change was not noted and therefore was not analyzed.

3 Discussion

3.1 Carbon foils discussion

In the case of non-irradiated graphene foil on electron microscope images, we can see the matrix in which the graphene structure is deposited. After irradiation, the absence of this matrix is visible and it probably melted by heat. EDS images before and after graphene irradiation no longer show elements other than before irradiation. Surface amorphization after irradiation is well visible on newly grown fibers on the surface. This decomposition of the matrix could cause a reduction in the efficiency of capturing the newly formed products. In contrast, graphene foil with an admixture of nanotubes showed more rugged and high-temperature resistance in the experiment. Non-irradiated graphene foil with nanotubes does not indicate any matrix presence, as was the case with pure graphene foils and higher carbon purity. After irradiation, the results do not differ significantly and we can state that the structure has been preserved. The reduction in efficiency can be attributed to the effect of irradiation, where there may have been more space in the structure due to collisions of newly formed products with the foilm. We can see surface changes before and after irradiation in Olympus digital microscope images, but these surface changes in nanotube-doped graphene do not interfere with the structure, which can be confirmed by XPS and XRD measurements, where the spectra have hardly changed. For graphene with a matrix, slight changes can be observed in both XPS and XRD.

3.2 Alluminium foils discussion

For EXP I, only foils No.3 and No.4 were analyzed, because foils No.1 and No.2 did not withstand the temperature effect due to their thickness and they tore and spread across the tube. For the aluminum foils No.3 and No.4, both the non-irradiated and the irradiated crystal structure was preserved (COD 4313217). In both cases, the irradiated foils have an uneven surface due to temperature and handling. On the irradiated foils, we can observe the temperature effect, which was achieved due to ion energy loss in material of the incoming beam with an energy of about 265 MeV. In the spectra from XPS measurements, we can observe that the non-irradiated foil is aluminum oxide, but the irradiated foil is only pure aluminum. Due to the temperature effect, the impurities evaporated.

3.2.1 Titanium and Nickel foils discussion

For EXP II, all foils except No.5 Ti were analyzed due to missing information. It is mentioned only in the initial setup of EXP II, but was not used during the experiment according to the journal 1, but its use in the experiment is obvious. Due to the absence of information on foil No.5, no analysis was performed, but measurements were performed. According to the journal, foil No.1 consisted of two foils, but there was only one in the experiment. We can only speculate whether it is a 2 or 3 μm foil, because measuring the thickness would be unreliable due to the creased surface. In the images from the Olympus digital microscope, we can observe small surface changes that could be caused by temperature effects. In the XRD spectrum of the irradiated foil, we can observe an additional 2 peaks. Non-irradiated foil No.1 has only the HCP structure (COD 9016190), which is characteristic of alpha titanium. In the irradiated foil, we can observe not only the HCP (COD 9016190) but also the BCC (COD 1534878) structure, which was formed due to the temperature effect during the experiment. In foil No.2, there was an unfortunate exchange of nickel for titanium. We can already observe a significantly different surface from the image from the digital microscope. This claim was supported by the EDS carried out in sector Ion-implantation nanotechnology and radiation materials science in FLNR JINR and also by the XRD, where the spectrum is completely different and no similarity is maintained. The relevant XRD software only identified the irradiated foil as titanium HCP (COD 9016190). An unirradiated No.2 nickel foil was identified as FCC (COD 4320489). The No.3 nickel foil in the Olympus digital microgroup shows a significant surface change. I believe that due to the temperature effect, growth of crystal grains. Furthermore, on the XRD spectra, a small peak was identified as glass, since it was too thin a foil that was on a glass substrate, the signal from the substrate could get into the XRD. Both unirradiated and irradiated nickel No.3 were identified by the FCC using XRD software (COD 4320489). Excluding this small deviation, the nickel foil before and after irradiation does not show any structural changes. Similarly to foil No.2, there was a confusion on foil No.4. Titanium was exchanged

for nickel here as in foil No.1 it is titanium HCP (COD 9016190) and in the irradiated foil similarly to foil No.3 it is FCC nickel (COD 4320489).

Conclusion

In the first part of the EXP I experiment, in the analysis of carbon foils, the probable cause of the low efficiency of the graphene foil (not) containing the matrix in which the graphene is deposited was found. In contrast, graphene foil with an admixture of nanotubes was a far better and more suitable candidate for the experiment not only because of its material stability during the experiment, but also due to its long-term efficiency. In the second part of EXP I, too thin aluminum foils proved unsuitable for reducing the energy of the ion beam. Aluminum foil with a thickness of 16,7 μm proved to be an ideal candidate for sufficient temperature resistance to reduce the energy of the ion beam. After irradiation, it remained in the form of pure aluminum. In EXP II, all foils have proven to be durable. However, the most interesting are titanium foils, which have a BCC structure. In summary, I would like to make recommendations when conducting experiments, so that careful records are made of the course of the experiment and changing the settings to avoid errors and inaccuracies.

References

[1] Boris Gikal, Igor Kalagin, Georgy Gulbekyan, Sergei Dmitriev, *STATUS OF THE FLNR JINR CYCLOTRONS*, Joint Institute for Nuclear Research, FLNR, Dubna, Moscow Region, Russia https://www.researchgate.net/publication/228696229_Status_of_the_FLNR_JINR_Cyclotrons [11.05.2022]

[2] https://accelconf.web.cern.ch/cyclotrons2016/talks/tha03_talk.pdf [11.05.2022]

[3] S.Bogomolov, V.Bekhterev, A.Efremov, B.Gikal, G.Gulbekian, Yu.Kostukhov, A.Lebedev, V.Loginov, N.Yazvitsky *RECENT DEVELOPMENT IN ECR ION SOURCES AT FLNR JINR*, Proceedings of RUPAC2012, Saint|-|Petersburg, Russia, 2012 https://www.researchgate.net/publication/290299062_Recent_development_in_ECR_ion_sources_at_FLNR_JINR [11.05.2022]

[4] A.S. Novoselov, A.M. Rodin, E.V. Chernysheva, S.N. Dmitriev, A.V. Gulyaev, A.B. Komarov, Yu.Ts. Oganessian, A.V. Podshibyakin. V.S. Salamatin, S.V. Stepantsov, V.Yu. Vedeneev, S.A. Yukhimchuk, L. Krupa, M. Holik, J. Kliman, D. Kamas, A. Opíchal, J. Pechousek, *Control and data acquisition systems of the MASHA setup*, Exotic Nuclei, pp. 427-430, 2019, https://www.worldscientific.com/doi/abs/10.1142/9789811209451_0060 [03.05.2022]

[5] V. Yu. Vedeneev, A. M. Rodin, L. Krupa, A. V. Belozerov, E. V. Chernysheva, S. N. Dmitriev, A. V. Gulyaev, A. V. Gulyaeva, D. Kamas, J. Kliman, A. B. Komarov, S. Motycak, A. S. Novoselov, V. S. Salamatin, S. V. Stepantsov, A. V. Podshibyakin, S. A. Yukhimchuk, C. Granja, S. Pospisil, *The current status of the MASHA setup*, Hyperfine Interactions volume 238, Article number:19, 2017, https://link.springer.com/article/10.1007/s10751-017-1395-9 [03.05.2022]

[6] A. M. Rodin, A. V. Belozerov, E. V. Chernysheva, S. N. Dmitriev, A. V. Gulyaev, A. V. Gulyaeva, M. G. Itkis, J. Kliman, N. A. Kondratiev, L. Krupa, A. S. Novoselov, Yu. Ts. Oganessian, A. V. Podshibyakin, V. S. Salamatin, I. Siváek, S. V. Stepantsov, D. V. Vanin, V. Yu. Vedeneev, S. A. Yukhimchuk, C. Granja, S. Pospisil, *Separation efficiency of the MASHA facility for short-lived mercury isotopes*, Hyperfine Interactions volume 227, pages 209–221, 2014, https://link.springer.com/article/10.1007/s10751-014-1010-2 [03.05.2022]

[7] https://interest.jinr.ru/uploads/report_files/report_student_92_project_34.pdf [11.05.2022]

[8] A. M. Rodin, A. V. Belozerov, D. V. Vanin, V. Yu. Vedeneyev, A. V. Gulyaev, A. V. Gulyaeva, S. N. Dmitriev, M. G. Itkis, J. Kliman, N. A. Kondratiev, L. Krupa, Yu. Ts. Oganessian, V. S. Salamatin, I. Sivacek, S. V. Stepantsov, E. V. Chernysheva, S. A. Yuchimchuk, *MASHA Separatoron the Heavy Ion Beam for Determining Masses and Nuclear Physical Properties of Isotopes of Heavy and Superheavy Elements*, Instruments and Experimental Techniques volume 57, pages 386–393, 2014, https://link.springer.com/article/10.1134/S0020441214030208 [03.05.2022]

[9] A. M. Rodin, V. Yu. Vedeneev, A. V. Gulyaev, M. Holik, D. Kamas, J. Kliman, A. B. Komarov, L. Krupa, A. S. Novoselov, A. Opíchal, J. Pechousek, A. V. Podshibyakin, V. S. Salamatin, S. V. Stepantsov, E. V. Chernysheva, S. A. Yukhimchuk, *Optimizing the Solid-State ISOL Technique for Separating Volatile Products of Complete Fusion Reactions*, Izvestiya Rossiiskoi Akademii Nauk, Seriya Fizicheskaya, 2020, Vol. 84, No. 4, pp. 553–558. https://www.researchgate.net/publication/341483460_Optimizing_the_Solid-State_ISOL_Technique_for_Separating_Volatile_Products_of_Complete_Fusion_Reactions [20.05.2022]

[10] Private concultation with MASHA group [03.09.2021 - 02.03.2022]

[11] Rodin A.M., Belozerov A.V., Dmitriev S.N., Itkis M.G., Kliman J., Krupa L., Lebedev A.N., Oganessian Yu.Ts, Salamatin V.S., Sivacek I., Vanin D.V., Chernyshova E.V., Yuchimchuk S.A. *Mass-spectrometer "MASHA" – complete assembly testing on heavy ion beam* [20.05.2022]

[12] KANEKA CORPORATION, http://www.elecdiv.kaneka.co.jp/english/graphite/ [12.01.2022] http://202.15.39.40/english/graphite/index_body.html [14.05.2022]

[13] Atsushi Tatami, Masamitsu Tachibana, Takashi Yagi, Mutsuaki Murakami *Preparation of Multilayer Graphene Sheets and Their Applications for Particle Accelerators*, American Institute of Physics
https://aip.scitation.org/doi/abs/10.1063/1.5035522 [20.05.2022]

[14] Applied Nanotech, Inc.
https://www.nanomagic.com/ani/ [12.01.2022]

[15] M. Mamatova, A. Seitkali, Eleonora Kudaibergenova, A. Rodin, L. Krupa, E. Chernysheva, V. Vedeneev, A. Novoselov, A. Podshibyakin, V. Salamatin, S. Stepantsov, A. Gulyaev, S. Yukhimchuk, A. Komarov, D. Kamas, A. Opíchal, J. Kliman *Study of Production Stability of Radon and Mercury Isotopes in Complete Fusion Reactions at the Mass- Separator MASHA by "Solid Hot Catcher" Technique*, AIP Conference Proceedings 2163, 070002 (2019)
https://aip.scitation.org/doi/abs/10.1063/1.5130114 [20.05.2022]

[16] http://www.crystallography.net/cod/4313217.html [23.05.2022]

[17] https://www.jp.xpssimplified.com/elements/aluminum.php [23.05.2022]

[18] http://www.crystallography.net/cod/9016190.html [23.05.2022]

[19] http://www.crystallography.net/cod/1534878.html [23.05.2022]

[20] http://www.crystallography.net/cod/4320489.html [23.05.2022]

[21] http://www.crystallography.net/cod/9008517.html [23.05.2022]

List of Figures

List of used symbols and shortcuts

JINR	Joint Institute for Nuclear Research
UPOL	Palacký University at Olomouc
KEF	Department of experimental physics
MASHA	Mass Analyter os Super Heavy Atoms
HSC	Hot Solid Catcher
F2C	Faraday Cap
ECR	Electron Cyclotron Resonance
RIBs	Radioactive Ion Beams
CNTs	Carbon NanoTubes
MLG	Multi-Layer Graphene
XPS	X-ray Photoelectron Spectroscopy
SEM	Scanning Electron Microscopy
TEM	Transmission Electron Microscopy
BF	Brightfield
EDS	Energy Dispersive Spectrometry
XRD	X-ray Diffraction Spectroscopy
COD	Crystallography Open Database
HCP	Hexagonal Close-Packed
FCC	Face centered cubic
BCC	Body centered cubic

Appendix 1 Photodocumentation

This appendix was created according to my intership to FLNR JINR. During my intership I created this documents and can help readers understand the experiment and calculations.

- Journal 0919 (EN).pdf (41 pages)
- Used foils for HSC and degrader.pdf (23 pages)
- Fluence MASHA EXP09191 I + HSC.xlsx (2 lists)
- Fluence MASHA EXP09191 II.xlsx (2 lists)